PRODUCTION AND CHARACTERIZATION OF ALUMINA AND CARBONYL IRON POWDER BASED SINTERED MAGNETIC ABRASIVE

Submitted by

ANUPAM ALOK
(Roll No. : **2K11/PIE/03**)
Mechanical Engineering Department

In partial fulfilment of the requirement of the degree of

MASTERS OF TECHNOLOGY

In

Production Engineering

Under the guidance of

Shri M. S. NIRANJAN

Assistant Professor

Department of Mechanical Engineering

DELHI TECHNOLOGICAL UNIVERSITY

(Formerly Delhi College of Engineering)

Bawana Road, New Delhi

JUNE 2013

CERTIFICATE

Date:-_____

This is to certify that report entitled **"PRODUCTION AND CHARACTERIZATION OF ALUMINA AND CARBONYL IRON POWDER BASED SINTERED MAGNETIC ABRASIVE"** by **Mr. ANUPAM ALOK,** is the requirement of the partial fulfilment for the award of Degree of **Master of Technology (M. Tech.)** in **Production Engineering** at **Delhi Technological University**. This work was completed under our supervision and guidance. He has completed his work with utmost sincerity and diligence. The work embodied in this project has not been submitted for the award of any other degree to the best of my knowledge.

(Guide)

MR. M.S. NIRANJAN

(ASSISTANT PROFESSOR)

(Co-Guide)

Dr. QASIM MURTAZA

(ASSOCIATE PROFESSOR)

DEPARTMENT OF MECHANICAL ENGINEERING

DELHI TECHNOLOGYCAL UNIVERSITY

DELHI

ACKNOWLDGEMENT

To achieve success in any work, guidance plays an important role. It makes us put right amount of energy in the right direction and at right time to obtain the desired result. I express my sincere gratitude to my supervisors, **Mr. M. S. NIRANJAN, Assistant Professor**, and **DR. QASIM MURTAZA, Associate Professor** Mechanical Engineering Department for giving valuable guidance during the course of this work, for their ever encouraging and timely moral support. Their enormous knowledge always helped me unconditionally to solve various problems.

I am greatly thankful to **Dr. NAVEEN KUMAR**, Professor and Head, Mechanical Engineering Department, Delhi Technological University, for his encouragement and inspiration for execution of the this work. I express my feelings of thanks to the entire faculty and staff, Department of Mechanical Engineering, Delhi Technological University, Delhi for their help, inspiration and moral support, which went a long way in the successful completion of my report work.

ANUPAM ALOK

(Roll No. 2K11/PIE/03)

ABSTRACT

This project focused on compacting, sintering and characterizing of Alumina and Carbonyl iron powder. Al_2O_3 -CIP composites containing equal volume fraction of Al_2O_3 and CIP were prepared through powder metallurgy method. Powder metallurgy method is well developed method of manufacturing ferrous and non ferrous parts. Solid and liquid phase sintering was done on high temperature tubular furnace in the inert atmosphere of argon. Solid phase sintering was done at 1000°C and liquid phase sintering was done at 1545°C in proper sintering cycle. After sintering, the sintered pallets are crushed using ball mill for obtaining the required size.

VSM is used to see the magnetization of the particles. The result shows that the saturation magnetization of sintered abrasive obtained at 9 ton compaction pressure is found to be highest. The different phases have been studied for all prepared samples using X-ray diffraction (XRD). The morphology and elemental composition as well as particle size has been studied using scanning electron microscope (SEM). Microstructure of samples has been studied using Optical microscope.

Compression strength test was done for all samples by universal testing machine (UTM). Bulk density of the pallets was calculated using standard Archimedean testing. The result showed that the bulk density value increases with compaction load. Micro hardness for samples was measured using micro-Vickers hardness instrument and pallets produced at compaction pressure of 9 ton shows highest hardness.

Keywords: Sintering, Carbonyl iron, Alumina, Magnetic Abrasive, Characterization.

CONTENTS

LIST OF FIGURE

LIST OF TABLES

NOMENCLATURE

PM	Powder Metallurgy
VOL	Volume
Al_2o_3	Aluminium Oxide (Alumina)
CIP	Carbonyl iron powder
°C	Degree Celsius
i.e.	That is
%	Percent
e.g.	Example
Wt	Weight
BHN	Brinell hardness number
D	Diameter
VHN	Vickers hardness number
Kgf	kilogram force
μ_m	Micrometers
KHN	Knoop hardness number
mm	Millimetre
MA	Magnetic abrasive
XRD	X-ray diffraction
UTM	Universal Testing Machine
VSM	Vibrating Sample Magnetometer
N	Newton

CRH	Constant rate heating
m	Meter
In	Inch
Å	Angstrom
ʎ	Wavelength

Chapter 1

INTRODUCTION

1. Introduction

Ceramics have been known to mankind since the earliest civilization and have played an important role in the evolution and development of human civilization. Generally ceramics are defined as solid crystalline materials composed of oxides, carbides, nitrides, borides having important structural, mechanical, thermal and electronic properties **[1]**. Metal matrix composites of iron with hard ceramic particles are of interest because of several advantages in terms of mechanical properties and easy fabrication. These materials are used in the aerospace, aircraft, automotive and many other manufacturing and industrial fields **[2-3]**. The technique that has consistently produced higher property composites has been powder metallurgy, which is competitive because of its low cost, ability to produce composites with high volume fraction, high productivity and possibility to fabricate components with complex geometry. Alumina is a technologically important material for electronic and structural applications. This is due to its superior thermal and physicochemical properties such as good creep strength, high hardness and high wear resistance, chemical inertness and resistance against high temperature corrosion as well as high electrical resistivity and high thermal conductivity, coupled with a reliable ceramic–metal joining technology. Alumina is an important structural ceramic material having many desirable properties like high melting point (2046 ±5°C), hardness (18GPa), elastic modulus (380GPa) and excellent resistance to acids and alkalis. It is being widely used as grinding media, textile thread guides, in paper manufacturing industry, cutting tools etc. However, it is brittle and has very low resistance to crack propagation i.e. low fracture toughness which results in catastrophic failure of the components. Recently, Nihara **[4]** has classified the ceramic matrix composites into four different categories (Fig. 1.1) on the basis of the matrix and reinforcement particle size. These are Intra-type; inter type, intra/inter-type and nano/nano-type. These nano composites show improved properties both at room temperature and at high temperature. The Hybridization of both micro-nano composites is expected to give further improvement. However the synthesis of nonmaterial's for bulk production is difficult due to grain growth of initial fine particles, introduction of processing related process flaws during initial sample preparation and handling of materials on its original dimension till the final microstructure development. These nano composites show improved properties both at room temperature and at high temperature. The hybridization of both micro-nano composites is expected to give further improvement. However the synthesis of nonmaterial for bulk production is difficult due to grain growth of

initial fine particles, introduction of processing related process flaws during initial sample preparation and handling of materials on its original dimension till the final microstructure development.

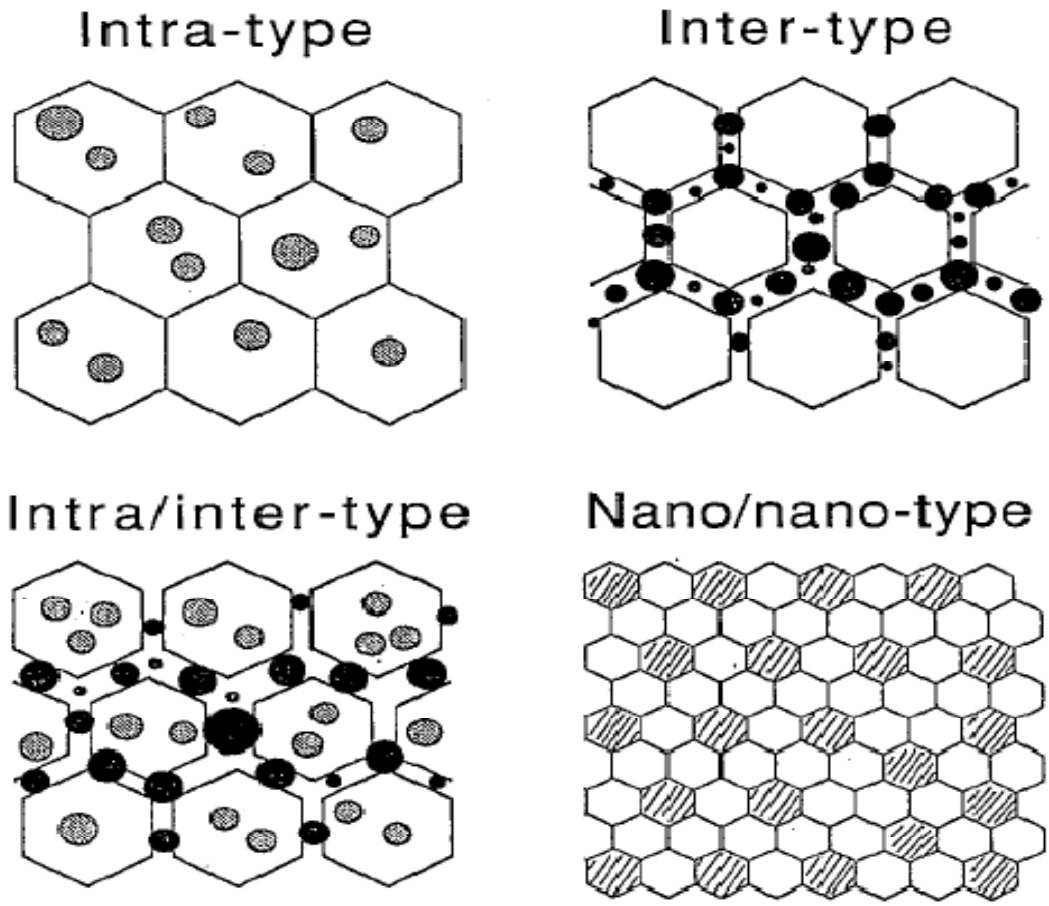

Fig. 1.1 Schematic representation of microstructure features of various nano composites as well as nano/nano composites

In today's technology the need of composite materials is very necessary due to the improve physical and mechanical properties. Iron has properties of specific saturation magnetization and it is a very soft magnetic material, low coactivity and a high Currie

temperature. A very highly pure iron is carbonyl iron powder and it is prepared by chemical decomposition of purified iron pent carbonyl. It usually has the appearance of grey powder, composed of spherical micro particles. Most of the impurities are carbon, oxygen, and nitrogen.

.

1.1 POWDER METALLURGY

Powder metallurgy (PM) is a metal working process for forming precision metal components from metal powders. The metal powder is first pressed into product shape at room temperature. This is followed by heating (sintering) that causes the powder particles to fuse together without melting. The parts produced by PM have adequate physical and mechanical properties while completely meeting the functional performance characteristics. The cost of producing a component of given shape and the required dimensional tolerances by PM is generally lower than the cost of casting or making it as a wrought product, because of extremely low scrap and the fewer processing steps. The cost advantage is the main reason for selecting PM as a process of production for high – volume component which needs to be produced exactly to, or close to, final dimensions. Parts can be produced which are impregnated with oil or plastic, or infiltrated with lower melting point metal. They can be electroplated, heat treated, and machined if necessary. The rate of production of parts is quite high, a few hundred to several thousand per hour. Industrial applications of PM parts are several. These include self – lubricating bearings, porous metal filters and a wide range of engineered shapes, such as gears, cams, brackets, sprockets, etc.

In the PM process the following three steps are followed in sequence: mixing (or blending), compacting, and sintering.

- Mixing: A homogeneous mixture of elemental metal powders or alloy powders is prepared. Depending upon the need, powders of other alloys or lubricants may be added.
- Compacting: A controlled amount of the mixed powder is introduced into a precision die and then it is pressed or compacted at a pressure in the range 100 MPa to 1000 MPa. The compacting pressure required depends on the characteristics and shape of the particles, the method of mixing, and on the lubricant used. This is generally done at room temperature. In doing so, the loose powder is consolidated and densified into a shaped model. The model is generally called “green compact.” As is comes out of the die, the

compact has the size and shape of the finished product. The strength of the compact is just sufficient for in – process handling and transportation to the sintering furnace.

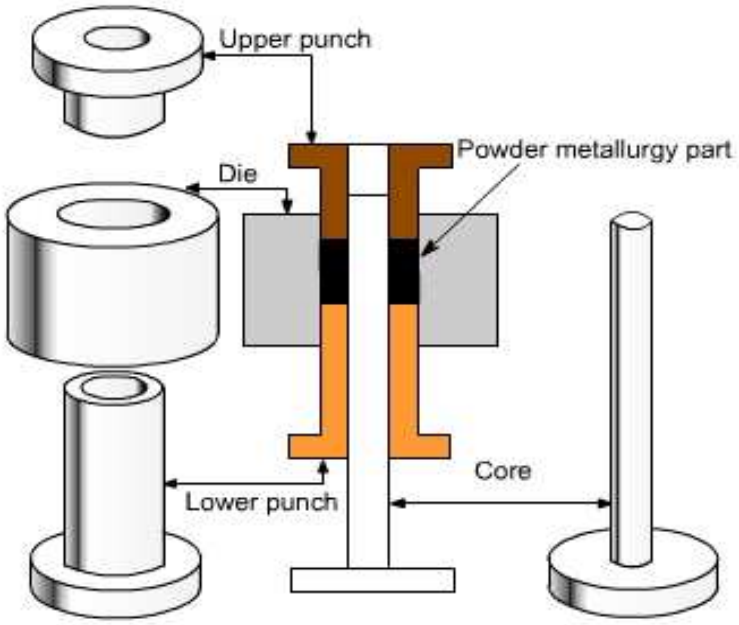

Fig 1.2 Typical set of powder metallurgy tools

- **Sintering:** During this step, the green compact is heated in a protective atmosphere furnace to a suitable temperature, which is below the melting point of the metal. Typical sintering atmospheres are endothermic gas, exothermic gas, dissociated ammonia, hydrogen, and nitrogen. Sintering temperature varies from metal to metal; typically these are within 70 to 90% of the melting point of the metal or alloy. Sintering is a solid state process which is responsible for producing physical and mechanical properties in the PM part by developing metallurgical bond among the powder particles. It also serves to remove the lubricant from the powder, prevents oxidation, and controls carbon content in the part. The structure and porosity obtained in a sintered compact depend on the temperature, time, and processing details. It is not possible to completely eliminate the porosity because voids cannot be completely closed by compaction and because gases evolve during sintering. Porosity is an important characteristic for making PM bearings and filters.

- Sometimes additional operations are carried out on sintered PM parts in order to further improve their properties or to impart special characteristics. Some important operations are as under.

1. Coining and sizing. These are high pressure compacting operations. Their main function is to impart (a) greater dimensional accuracy to the sintered part, and (b) greater strength and better surface finish by further densification.
2. Forging. The sintered PM parts may be hot or cold forged to obtain exact shape, good surface finish, good dimensional tolerances, and a uniform and fine grain size. Forged PM parts are being increasingly used for such applications as highly stressed automotive, jet – engine and turbine components.
3. Impregnation. The inherent porosity of PM parts is utilized by impregnating them with a fluid like oil or grease. A typical application of this operation is for sintered bearings and bushings that are internally lubricated with up to 30% oil by volume by simply immersing them in heated oil. Such components have a continuous supply of lubricant by capillary action, during their use. Universal joint is typical grease – impregnated PM part.
4. Infiltration. The pores of sintered part are filled with some low melting point metal with the result that part's hardness and tensile strength are improved. A slug of metal to be impregnated is kept in close contact with the sintered component and together they are heated to the melting point of the slug. The molten metal infiltrates the pores by capillary action. When the process is complete, the component has greater density, hardness, and strength. Copper is often used for the infiltration of iron – base PM components. Lead has also been used for infiltration of components like bushes for which lower frictional characteristics are needed.
5. Heat Treatment. Sintered PM components may be heat treated for obtaining greater hardness or strength in them.
6. Machining. The sintered component may be machined by turning, milling, drilling, threading, grinding, etc. to obtain various geometric features.
7. Finishing. Almost all the commonly used finishing method is applicable to PM parts. Some of such methods are plating, burnishing, coating, and colorings.

Plating - For improved appearance and resistance to wear and corrosion, the sintered compacts may be planted by electroplating or other plating processes. To avoid penetration and entrapment of plating solution in the pores of the part, an impregnation or infiltration treatment is often necessary before plating. Copper, zinc, nickel, chromium, and cadmium plating can be applied.

Burnishing - To work harden the surface or to improve the surface finish and dimensional accuracy, burnishing may be done on PM parts. It is relatively easy to displace metal on PM parts than on wrought parts because of surface porosity in PM parts.

Coating - PM sintered parts are more susceptible to environmental degradation than cast and machined parts. This is because of inter – connected porosity in PM parts. Coatings fill in the pores and seal the entire reactive surface.

Colouring - Ferrous PM parts can be applied colour for protection against corrosion. Several methods are in use for colouring. One common method to blacken ferrous PM parts is to do it chemically, using a salt bath.

8. Joining - PM parts can be welded by several conventional methods. Electric resistance welding is better suited than oxy- acetylene welding and arc welding because of oxidation of the interior porosity. Argon arc welding is suitable for stainless steel PM parts.

1.2 MOTIVATION AND OBJECTIVES

In the present scenario, demand of magnetic abrasive is very high for finishing purpose in the electronics and aero space industries. This project focused on Production, testing & characterization of alumina and carbonyl iron powder based sintered magnetic abrasives. Carbonyl iron powder and alumina are mixed in 20 vol % each in ball mill and pallets are prepared with 5 g weight mixture at 5 ton, 7 ton, 9 ton compacting pressure with 15 min. holding time. Powder metallurgy process is used to produce the pellets for sintering in a specified sintering cycle. After sintering, the component is again milled using ball mill to produce micron sized particle of magnetic abrasive powder. Characterization of the powder (particle size, shape etc) has been studied by XRD, SEM techniques and Magnetic properties were tested by Vibration sample magnetometer.

Chapter II

Literature Review

2. Literature Review

Rahimian, M. et al. (2009) [5]. The aim of this paper was to investigate the effect of alumina particle size, sintering temperature and sintering time on the properties of Al–Al_2O_3 composite. The average particle size of alumina was 3, 12 and 48μm. Sintering temperature and time were in the range of 500–600°C for 30–90 min. A correlation was established between the microstructure and mechanical properties. The investigated properties include density, hardness, microstructure, yield strength, compressive strength and elongation to fracture. It was concluded that as the particle size of alumina is reduced, the density is increased followed by a fall in density. In addition, at low particle size, the hardness and yield strength and compressive strength and elongation to fracture were higher, compared to coarse particles size of alumina. The variations in properties of Al–Al_2O_3 composite are dependent on both sintering temperature and time. Prolonged sintering times had an adverse effect on the strength of the composite. Result show the relative density of Al–Al_2O_3 composite was higher in samples containing fine particle sizes. The highest relative density of 99.95% was observed in specimens sintered at 600°C. The grain size of samples having fine Al_2O_3 particles is smaller and increasing the sintering time to 90min leads to grain coarsening. The highest hardness was 76HB in specimens containing average particle size of 3μm sintered at 600 ◦C for 45 min. Further increase in sintering time to 90min results in a reduction in hardness to 59 HB. The finer the particle size of alumina, the greater the compressive strength and elongation. The highest strength was 318MPa, for the composite containing an average particle size of 3μm and sintered at 600 ◦C for 45 min. Further increase in sintering time has an adverse effect on the strength. Extended sintering times and also the use of fine alumina in Al–Al_2O_3 composite results in higher elongations. Maximum elongation was observed to be 61.8% in samples containing the average particle size of 3μm.

Shamsuddin, Saidatulakmar et al.(2008) [6] this paper focused on fabricating and characterizing composites of iron-chromium alloy reinforced with 5–25 wt. % of alumina particles fabricated using powder metallurgy method. The diffraction patterns of X-Ray diffraction (XRD) reveal the influence of varying weight percentage of alumina. Comparisons on the mechanical properties are also being made on the unreinforced iron matrix (0 wt. %). The compatibility between matrix and reinforcement was indicated from the microstructure

examination showing homogeneous distribution of alumina particles in the alloy matrix. Bulk density and porosity of the composites were calculated using standard Archimedean testing. Micro-hardness was measured using micro-Vickers hardness instrument. The data obtained showed that the 20 wt. % alumina produced the highest hardness reading.

Tartaj P. and Tartaj J. (2002), [7] the purpose of this paper was to preparation of homogeneous iron oxide doped alumina spherical particles. The method is based on the hydrolysis with ammonium hydroxide of liquid aerosols formed by spraying iron and alumina nitrate aqueous solutions. The powder consisted of, according to X-ray diffraction and infrared spectroscopy, boehmite of low crystalline. Heating of the as-prepared boehmite powders produced a series of transition alumina that finally transform into the thermodynamically stable phase (α-Al2O3).

LU C. Y. and HWANG S. K. (1999) [8] this paper focused on the effect of alumina particles on the sintering behaviour of a carbonyl iron powder compact. Two different-sized alumina, 0.05 and 0.4 mm, were mixed with the iron compact at amounts up to 1.2 wt pct. When 0.4mm alumina particles were added, no sintering enhancement was observed. With 0.1 wt pct, the sintered density increased from 7.25 to 7.40 g/cm3 after the compact was sintered at 1350 8C for 1 hour in hydrogen. Dilatometric curves showed that alumina impeded the early-stage sintering of iron in a phase, but improved densification in the g phase at high temperatures. These results, along with micro structural analysis, suggested that alumina particles exhibit dual roles; their physical presence blocks the diffusion of iron atoms, thus causing inhibition of sintering, while their grain boundary pinning effect prevents exaggerated grain growth of iron and helps densification. It follows that, depending upon the amount and size of the alumina powders, either an increase or decrease in the final sintered density can be obtained.

Chen Lung Chih et al.(2002) [9] the purpose of this paper was using metal-organic chemical vapour infiltration (MOCVI) conducted in fluidized bed was employed for the preparation of nano-sized ceramic composites. The Cr-species was infiltrated into Al2O3 granules by the pyrolysis of chromium carbonyl (Cr (CO)6) at 300–450°C. The granulated powder was pressure less sintered or hot-pressed to achieve high density. The results showed that the dominant factors

influencing the Cr-carbide phase formation, either Cr3C2 or Cr7C3, in the composite powders during the sintering process were the temperature and oxygen partial pressure in the furnace. The coated Cr-phase either in agglomerated or dispersive condition was controlled by the use of colloidal dispersion. The microstructures showed that fine (20 – 600 nm) CrxCy grains (_8 vol. %) located at Al2O3 grain boundaries hardly retarded the densification of Al2O3 matrix in sintering process. The tests on hardness, strength and toughness appeared that the composites with the inclusions (Cr3C2) had gained the advantages over those by the rule of mixture. Even 8 vol.% ultrafine inclusions have greatly improved the mechanical properties. The strengthening and toughening mechanisms of the composites were due to grain-size reduction, homogenous dispersion of hard inclusions, and crack deflection.

Olevsky A. Eugene (1997) [10] focused on Theoretical concepts of sintering were originally based upon ideas of the discrete nature of particulate media. However, the actual sintering kinetics of particulate bodies are determined not only by the properties of the particles themselves and the nature of their local interaction with each other, but also by macroscopic factors. Among them are externally applied forces, kinematic constraints *(*e.g. adhesion of the sample's end face and furnace surface*)*, and in homogeneity of properties in the volume under investigation *(*e.g. in homogeneity of initial density distribution created during preliminary forming operations*)*. Insufficient treatment of the questions enumerated above was one of the basic reasons hindering the use of sintering theory. A promising approach is connected with the use of continuum mechanics, which has been successfully applied to the analysis of compaction of porous bodies. This approach is based upon the theories of plastic and nonlinear-viscous deformation of porous bodies. Similar ideas have recently been embodied in a continuum theory of sintering. The main results of the application of this theory for the solution of certain technological problems of sintering are introduced including their thermo–mechanical aspects.

Park, H. H. et al. (1984) [11] In this paper models for liquid flow into isolated pores during liquid phase sintering are described qualitatively. The grains are assumed to maintain an equilibrium shape determined by a balance between their tendency to become spherical and a negative capillary pressure in the liquid due to menisci at the specimen surface and the pore. With an increase of grain size, the grain sphering force decreases while the radius of liquid menisci increases to maintain the force equilibrium. When grain growth reaches a critical point,

the liquid menisci around a pore become spherical and the driving force for filling the pore rapidly increases as liquid flows into it. The critical grain size required for filling a pore increases linearly with pore size. Experimentally, filling of isolated pores has been investigated in Fe-Cu powder mixture after liquid phase sintering treatment and after dipping into a molten matrix alloy. The observed pour filling behaviours agree with the qualitative predictions based on the models. In Fe-Cu alloy, pour filling is terminated by gas bubbles formed in liquid pockets. By focusing on the evolution of pores during liquid phase sintering, it was demonstrated that pores are filled by liquid flow after a critical incubation time during sintering. Theoretical analysis shows that the critical condition for pour filling is satisfied when the grains grow to a certain size. The concept of the critical grain size hinges upon the equilibrium between the grains and the liquid menisci. In a fully densified specimen with a limited liquid content, the grains are kept in the anhedral (contact flattened) shape by the liquid menisci at the specimen surface which act against the tendency of the grains to become spherical. As the grains grow, the sphering force will decrease, and the menisci radius will increase until it becomes equal to the radius of a pore which may be present. A description of the pour filling process in a system which contains many pores of different size will be more complex. In this study the grain shape was assumed to be always at the local equilibrium state determined by the liquid volume fraction. If the grain shape deviates from the local equilibrium state, an imbalance between the sphering force and the liquid pressure will appear and induce a grain shape change. The kinetics of this grain shape change is, of course, a separate problem. This study also demonstrates that liquid, flowing rapidly under the capillary pressure, can introduce a greater non uniformity in the structure compared to that encountered in solid state sintering. Therefore, any model based on a uniform structure such as the two particle model cannot completely describe the liquid phase sintering process. The grain shape at local equilibrium is influenced by the dihedral angle, and the meniscus geometry is strongly dependent on the assumed shape of the grain at the specimen surface.

2.1 Powder Sintering

In ceramic manufacturing, sintering is a high temperature process which converts loosely bound particle compact in to a dense and cohesive body with a fine grained microstructure. This is usually achieved only when pores are uniformly distributed on grain boundaries which facilitate

pore annihilation during final stage of sintering and avoids rapid grain growth **[12, 13].** Usually a green compact made from an initial small particle size and narrow pore size distribution usually **[14-18]** sinters to a uniformly dense body. Agglomerated powder **[17-19]** on the other hand, disrupts the particle packing and produce a spatially heterogeneous green microstructure – a situation usually observed with nano powder compaction. Such an inhomogeneous microstructure affects densification kinetics as well as the final sintered density achievable **[19-21].** Sinter ability could also be improved by controlling the agglomeration tendency during powder processing. The elimination of agglomerates by colloidal processing produces homogeneously packed green microstructure which could be sintered to high density at lower sintering temperature. Besides colloidal processing, two step sintering process can also produce a high density, fine grain size sintered body [**22-23**]. The production of dense ceramics from nano crystalline powders requires clear understanding of the fundamental sintering theory as well as sintering models. Densification and microstructure evolution are interdependent and the densification process is influenced by the mechanism, material transport paths, material flux and mass transport distance. An excellent review by Exner discusses the initial stage of sintering kinetics and the controlling parameters. The particle – particle contact during sintering require simple geometrical assumptions for neck area, volume, radius of curvature and diffusion distance. The early models assumed several simple geometric approximations and ignored the possibility of multiple or parallel material transport paths. These simplified assumptions were less accurate when compared with the rigorous mathematical treatments obtained with exact neck shape. However, numerical analysis of the geometrical changes during sintering has been subject to criticism. In the past, isothermal study was the major source of sintering data many of which did not agree well with the theoretical predictions. The discrepancy was partially due to the finite time required for reaching the isothermal sintering temperature and various corrections incorporated in the sintering result to account for the transient events during heating. Two key decisions were made in an effort to minimize the experimental errors. Firstly, the use of constant heating rate measurements for establishing the initial events which did not require time or temperature corrections during the heating cycles and secondly, both shrinkage and surface area were measured to monitor the geometric changes and sintering mechanisms. On the other hand, constant rate heating (CRH) method required lesser experimental work. In a single experiment involving slower heating rates, the temperature variation was less across a wide range and steady

state could be reached at every temperature. Several methods had been used for the kinetic parameter calculation from the sintering curves obtained at different linear heating rates. The initial stage sintering activation energy had been obtained from the Arrhenius plots of the shrinkage rate (or densification rate) at equal values of the shrinkage (or density).

Chapter III

MECHANICAL TESTING AND CHARACTRIZATION

3. Mechanical testing and characterization

Mechanical properties of P/M structural materials depend on the composition, density, and heat treatability of the material, as well as processing and design considerations. Fabricated P/M parts are evaluated and tested at several stages during the manufacturing for part acceptance and process control. This can include various types of tests, such as:

- Evaluation of dimensional changes
- Hardness/Micro hardness testing
- Strength testing
- Wear testing
- Optical properties testing (Roughness)
- Crack detection

3.1 Dimensional evaluation

During the manufacture of sintered parts, dimensional change must be accommodated for during each processing step. Causes of these changes include:

- Elastic spring back during ejection from tooling used for cold pressing
- Growth or shrinkage during delubrication, pre sintering, and sintering
- Elastic spring back from tooling during cold repressing or sizing
- Thermal contraction from the tools used in hot forging or hot repressing
- Tool wear in cold or hot compacting
- Machining tolerances at secondary machining and associated tool wear
- Distortion during annealing
- Growth or shrinkage during carburizing, nitriding, or neutral hardening
- Shrinkage during tempering
- Growth during steam blackening

3.2 Measurement of density

Density is the ratio of mass to volume. For a given material, degree of sintering, and heat treatment, density determines mechanical and physical properties. For example, higher density in sintered steels results in higher tensile strength, elongation, and impact resistance values.

Methods based on Archimedes' principle- Typical methods of measuring density depend on Archimedes' principle, in which hydrostatic forces in liquids exert buoyant forces proportional to the part volume. This measurement is standardized in ASTM B 328, MPIF test method 42, and International Standards Organization test method ISO 2738.

When an object is immersed in a liquid, the liquid exerts an upward buoyant force that is equal to the product of the object volume and the density of the liquid.

Density= mass/▲v.

Where ▲v = final volume- initial volume

3.3 Hardness and micro hardness

Porous materials exhibit wider variation in hardness testing than wrought counterparts. The entrance of the indenter into pores or groups of pores generally causes this effect. At least five consistent readings should be taken, in addition to any obviously high or low readings, which are discarded. The remaining five readings should be averaged.

Hardness: The hardness of a material is related to the resistance to indentation. This property is useful for studying the strength and heat treatments carried out on materials. Depending on the test conducted 3 types of hardness measurements are classified as scratch hardness, indentation hardness and rebound or dynamic hardness. For metals and ceramics indentation hardness is most common.

Brinell hardness test: In the Brinell test, a hardened steel ball is pressed for 10-15 s on the surface of the material by standard load. After the load and ball have been removed, the diameter of the indentation is measured. Brinell hardness number (BHN) is given as

$$BHN = \frac{P}{\left(\frac{\pi D}{2}\right)\left(D-\sqrt{(D^2-d^2)}\right)}$$

Where P= applied load

D= diameter of ball in mm

D= diameter of indentation in mm

Vickers hardness test: This test involves a diamond indenter, in the form of a square pyramid with an apex angle of 136°, being pressed under load for 10-15s into the surface of the material under test. Vickers hardness number (HV) is obtained by dividing the applied load by surface area (mm^2) of the indentation.

$$Area\ of\ indentation = \frac{d^2}{2Sin\frac{\theta}{2}} = \frac{d^2}{1.854}$$

Where d= mean diagonal length

2θ = apex angle (136°)

$$HV = \frac{1.854P}{d^2}$$

Rockwell hardness test: This test utilizes the depth of indentation under constant load as a measure of hardness. The Rockwell scale is a hardness scale based on the indentation hardness of a material. The Rockwell test determines the hardness by measuring the depth of penetration of an indenter under a large load compared to the penetration made by a preload. There are different scales, denoted by a single letter, that use different loads or indenters. The result is a dimensionless number noted as HRA, where A is the scale letter.

When testing metals, indentation hardness correlates linearly with tensile strength. This important relation permits economically important non destructive testing of bulk metal deliveries with lightweight, even portable equipment, such as hand-held Rockwell hardness testers

Micro hardness test: The term micro hardness test usually refers to static indentations made with loads not exceeding 1 kgf. The indenter is either the Vickers diamond pyramid or the Knoop elongated diamond pyramid. The procedure for testing is very similar to that of the standard Vickers hardness test, except that it is done on a microscopic scale with higher precision instruments. The surface being tested generally requires a metallographic finish; the smaller the load used, the higher the surface finish required. Precision microscopes are used to measure the indentations; these usually have a magnification of around X500 and measure to an accuracy

of ±0.5 micrometres. Also with the same observer differences of ±0.2 micrometres can usually be resolved. It should, however, be added that considerable care and experience are necessary to obtain this accuracy.

The Knoop hardness number KHN is the ratio of the load applied to the indenter, P (kgf) to the unrecovered projected area A (mm^2)

$$KHN = \frac{P}{A_p} = \frac{P}{CL^2}$$

Where F= applied load in kgf

A = the unrecovered projected area of the indentation in mm^2

L = measured length of long diagonal of indentation in mm

C = Constant of each indenter supplied by each manufacturer

3.4 Strength testing

Compressive strength: The compressive strength of a material is a measure of its ability to bear crushing or pressing loads. The compressive strength of a material is given by

$$S = \frac{P}{A}$$

Where P= load at fracture

A= Cross sectional area of the test piece

A lot of care is required in specimen preparation and alignment. The specimen faces bearing the load must be absolutely flat and parallel.

Characterization of Powders

Particle size and size distribution have a significant effect on the behavior of metal powders during processing; thus to a considerable extent, they govern the properties of the final products made from powder. Consequently, characterization of such properties is essential. In the P/M industry, the traditional and most widely used method of particle size measurement is sieving. Sieves or screens are used not only for particle size measurement, but also for separation of powder into different sieve fractions.

This twofold use of sieves, in addition to the fact that most P/M powders are -80 meshes (smaller than about 180 m in diameter, with only minor amounts smaller than 10 m) has been well suited to industrial applications. For powders with large percentages of -400 mesh 38 m) particles, sieve distribution data are often complemented with other particle size measuring instruments.

Sieve designation, mesh	Sieve openings	
	μm	in.
30	600	0.0232
40	425	0.0164
50	300	0.0116
60	250	0.0097
80	180	0.0069
100	150	0.0058
140	106	0.0041
200	75	0.0029
230	63	0.0024
325	45	0.0017

Table 3.1 Standard U.S. sieve series

3.5 X-Ray powder diffraction

X-ray powder diffraction (XRPD) techniques are used to characterize samples in the form of loose powders or aggregates of finely divided material. These techniques cover various investigations, including qualitative and quantitative phase identification and analysis, determination of crystalline, micro identification, lattice-parameter determinations, high temperature studies, thin film characterization, and, in some cases, crystal structure analysis. The powder method, as it is referred to, is perhaps best known for its use as a phase characterization tool partly because it can routinely differentiate between phases having the same chemical

composition but different crystal structures (polymorphs). Although chemical analysis can indicate that the empirical formula for a given sample is FeTiO3, it cannot determine whether the sample is a mixture of two phases (FeO and one of the three polymorphic forms of TiO2) or whether the sample is the single-phase mineral FeTiO3 or ilmenite. The ability of XRD to perform such identifications more simply, conveniently, and routinely than any other analytical method explains its importance in many industrial applications as well as its wide availability and prevalence.

In general, an x-ray powder diffraction characterization of a substance consists of placing a powder sample in a collimated monochromatic beam of x-radiation. The diffraction pattern is recorded on film or using detector techniques, then analyzed to provide x-ray powder data that can be used to solve such problems. In XRD analysis, samples usually exist as finely divided powder (usually less than 44μ m in size) or can be reduced to powder form. The particles in a sample comprise one or more independently diffracting regions that coherently diffract the x-ray beam. These small crystalline regions are termed crystallites. Consolidated samples, such as ceramic bodies or as-received metal samples will likely have crystallites small enough to be useful for powder diffraction analysis, although they can appear to have considerably larger particle sizes. This occurs because a given grain or particle can consist of several crystallites (independently diffracting regions). Although larger grain sizes can sometimes be used to advantage in XRD, the size limitation is important because most applications of powder diffraction rely on x-ray signals from a statistical sample of crystallites. The angular position θ, of the diffracted x-ray beam depends on the spacing's, *d,* between planes of atoms in a crystalline phase and on the x-ray wavelength λ:

$N\lambda = 2d\sin\theta$

A diffraction pattern can be recorded using film, analog, or digital methods. Whether film, analog or digital data collection is used, the final data can be displayed as a graph of intensity, as a function of inter planar distance *d,* or as a function of diffraction angle 2θ. Many modem automated powder diffracto meters can provide further data reduction, including peak finding. A tabular listing of peak intensity versus inters planar spacing, search/match software, and other computer utilities.

3.6 Transmission electron microscopy

The transmission electron microscope is used for counting particles that range from 0.001 to 5µ m in diameter. This instrument has a large depth of field; consequently, all particles in the field of view are in focus regardless of size. Particles are usually not counted directly from the viewing screen of the transmission electron microscope. Photographs are normally taken, and counts are made from prints or projected images using the negatives.

The electron beam is easily absorbed, and films greater than 100 to 200 nm (1000 to 2000Å) is completely opaque. It is therefore necessary to produce very thin support films on which powders can be dispersed for counting. These films usually are made of carbon. One of the best techniques for producing strong, flat carbon support films involves cleaving high-quality mica and placing it immediately in a vacuum evaporation unit. After a hard vacuum has been obtained, carbon is evaporated onto the mica surface to a thickness of about 10 nm (100 Å). Powders are dispersed on the surface of support films by puffing from an aspirator or by allowing a drop of aqueous suspension to dry. Carbon films are hydrophobic; use of an aqueous suspension requires that they be rendered hydrophilic by either treatment with a thin solution of albumen or exposure to reactive oxygen in a low-temperature oxygen Asher.

Exposure to reactive oxygen must be done at a very low setting (4 W) for several seconds, or the carbon film will be destroyed.

Particle thicknesses can be measured in the transmission electron microscope by "shadowing" particle dispersions in which the particles sit on a substrate and are not embedded in a plastic film. This is done by evaporating a small amount of metal placed at an angle to the substrate surface in a vacuum chamber. The metal coats the surface and particles in a line-of-sight fashion, leaving a "shadow" cast behind the particles. Commercially available precision-sized latex spheres can be included with the powder sample so that the shadow length to particle height ratio can be calculated.

3.7 Scanning electron microscopy

The scanning electron microscope has a resolution of about 10 nm (100 Å) and is capable of very low magnification (about 10×) up to about 50,000×. It therefore can be used to count particles ranging in size from 1 mm to 0.1µ m. Particles smaller than 0.1µ m usually have too low a

contrast with the background to be counted efficiently. The scanning electron microscope has about 300× the depth of field of an optical microscope. The image in the scanning electron microscope usually is obtained by using the secondary electron output of the sample as it is scanned by a very narrow electron beam. The contrast of the image depends more on the topography of the sample than on differences in atomic number. Therefore, prepared powders must not be embedded in films, but dispersed on a smooth substrate. Any smooth surface can be used as a substrate. However, if energy dispersive x-ray analysis (EDXA) is to be performed for particle identification, a carbon or polystyrene surface is preferred.

An excellent substrate can be made by placing a polystyrene pellet on a glass slide and heating it on a hot plate until it softens. A second glass slide is then placed over this slide and pressed until the pellet forms a thin disk. The slides are removed from the hot plate and pressed together until the polystyrene sets. The disk thus formed is as smooth as the glass and contains no elements that may hinder EDXA. For sample preparations using aqueous suspensions, polystyrene surfaces can be rendered hydrophilic by a brief treatment in oxygen Asher at low power (5 to 10 W for 5 s). While the substrates for SEM do not have to be as thin as those used for TEM, they must be conductive. Consequently, if glass or plastic surfaces are to be used, they must be coated with an evaporated metal (or carbon, for EDXA) film. This coating is usually applied after the particles have been dispersed on the surface. Many of the dispersing techniques used for TEM can be applied to SEM. Particle dusting, drying from liquid suspensions, and mulling in liquids that can be sublimed in a vacuum are suitable dispersing methods, depending on the powder. If the technique of mulling in parlodion and amyl acetate is used, parlodion can be removed in an oxygen Asher, thus leaving the particles on the substrate. Suitable substrates include glass or metal, because they are not affected by the aching. The prepared sample should always be placed in the scanning electron microscope with the surfaces normal to the electron beam so that the magnification, which changes with working distance, will be the same on all areas of the viewing screen. Particle counting can be done directly from the viewing screen, from photographs, or by using an automatic image analyzer.

3.10 Vibrating sample magnetometer

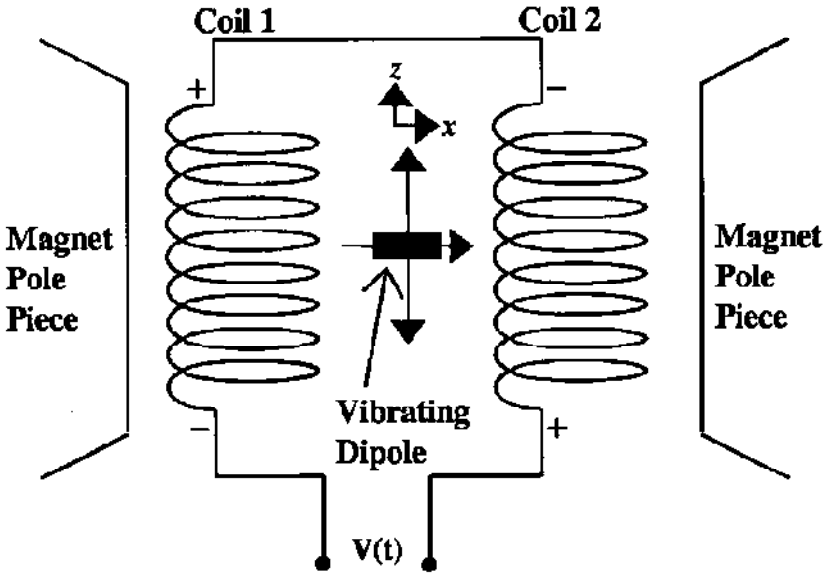

Fig. 3.1 working principle of VSM.

The VSM is based upon Faraday's law according to which an *e.m.f.* is induced in a conductor by a time-varying magnetic flux. In VSM, a sample magnetized by a homogenous magnetic field is vibrated sinusoid ally at small fixed amplitude with respect to stationary pick-up coils. The resulting field change **B** (*t*) at a point **r** inside the detection coils induces voltage and is given by

$$v(t) = \sum_{n} \int_{A} \frac{\partial B(t)}{\partial t} . dA$$

Where **A** is the area vector of a single turn of the coil and the summing is done over *n* turns of the coils. **B** (*t*) is given by the dipolar approximation, assuming small dimensions of the magnetized sample in comparison to its distance from the detection coils,

$$B(r) = \frac{\mu_o}{4\pi}\left(\frac{m}{r^3} - \frac{3(m.r)r}{r^3}\right)$$

and

$$\frac{\partial B_i(t)}{\partial t} = \frac{\partial a(t)}{\partial t} . \underset{\nabla}{\rightarrow} \{B(r)\}_i$$

a(t) being the position of the dipole and $\{B(r)\}i$, i = 1, 2, 3, the ith component of **B** at **r** due to dipole **m**. $V(t)$ can be detected to a high resolution and accuracy by means of suitable associated electronics. For stationary pick-up coils and a uniform and stable external field, the only effect measured by the coils is that due to the motion of the sample. The voltage V (t) is thus a measure of the magnetic moment of the sample.

Chapter IV

Experimental Work

4.1 selection of powder

To make magnetic abrasive powder, two abrasive powders, Alumina and Carbonyl Iron Powder is selected as Magnetic component of MA powder.

4.2 Mixing

Mixing purpose was done by ball mill with steel ball. For mixing purpose powder was taken in equal proportion i.e. 20% volume of alumina and 20% volume of carbonyl iron powder.

Fig 4.1 Ball Milling machine

4.3 Compacting

For compacting purpose use a 12 ton capacity hydraulic jack with 13 mm die. For compacting purpose take 5gm powder and make pallets of 5 ton, 7 ton and 9 ton. For each pallets take holding time is 15 mins.

Fig 4.2 Hydraulic Jack with die

4.4 Sintering

Solid phase and Liquid phase sintering is done in High temperature tube furnace, having capacity up to 1600°C. Inert environment of Argon is used to avoid any kind of atmospheric contamination. The most important factors involved during the sintering process are temperature, time and furnace atmosphere. Increasing the sintering temperature greatly increases the rate and magnitude of any change in the properties occurring during the sintering. Here maximum temperature is used for solid sintering is 1000°C and for liquid phase sintering maximum temperature is 1545°C. Here temperature rate is 3°C/min and cooling rate is 6°C/min. Two type of sintering cycle is used for sintering one for solid phase and another for liquid phase sintering.

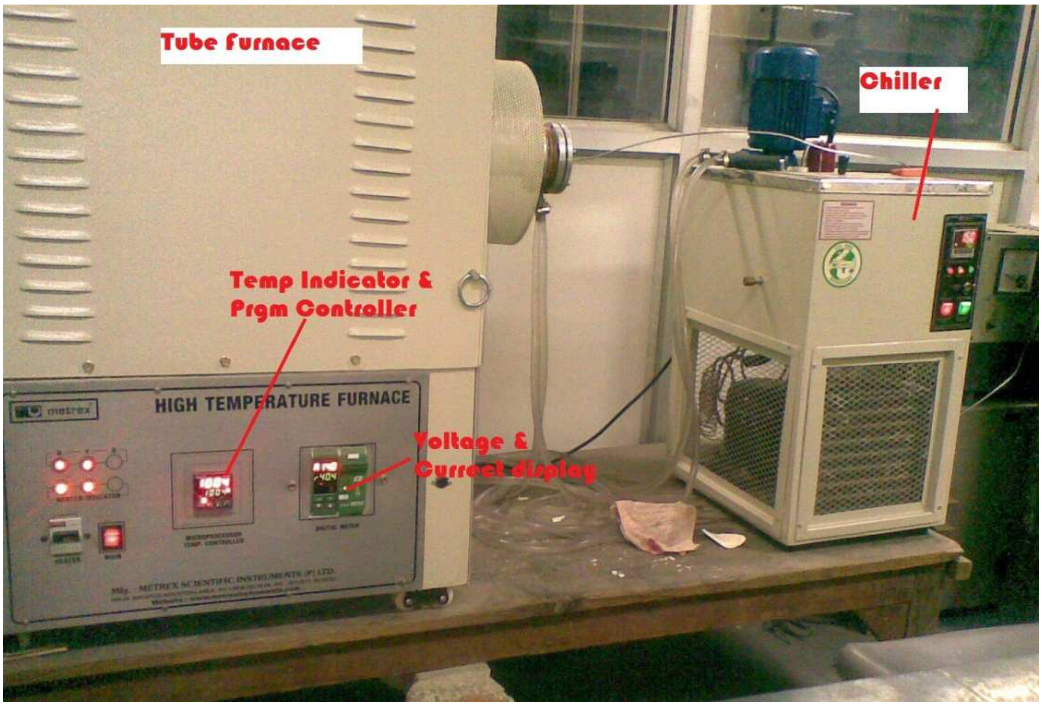

Fig 4.3High temperature tube furnace

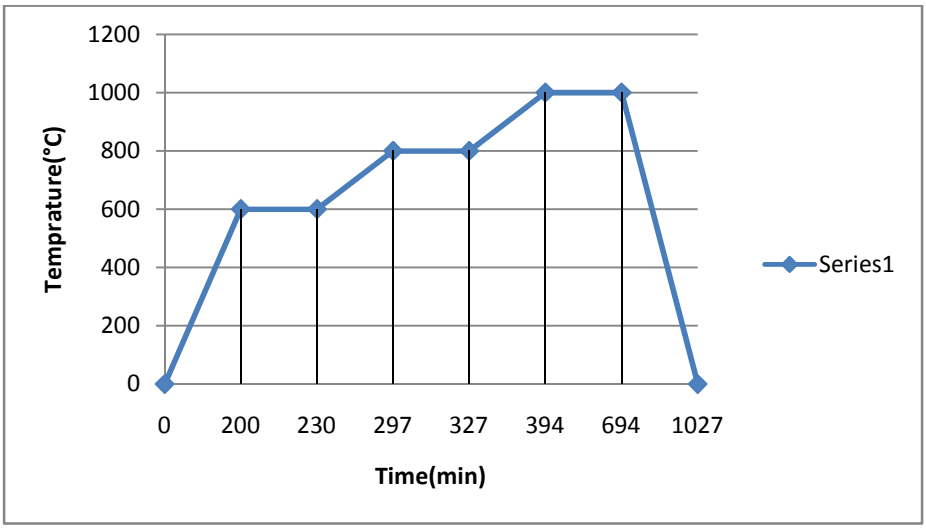

Fig. 4.4 sintering cycle for solid phase sintering

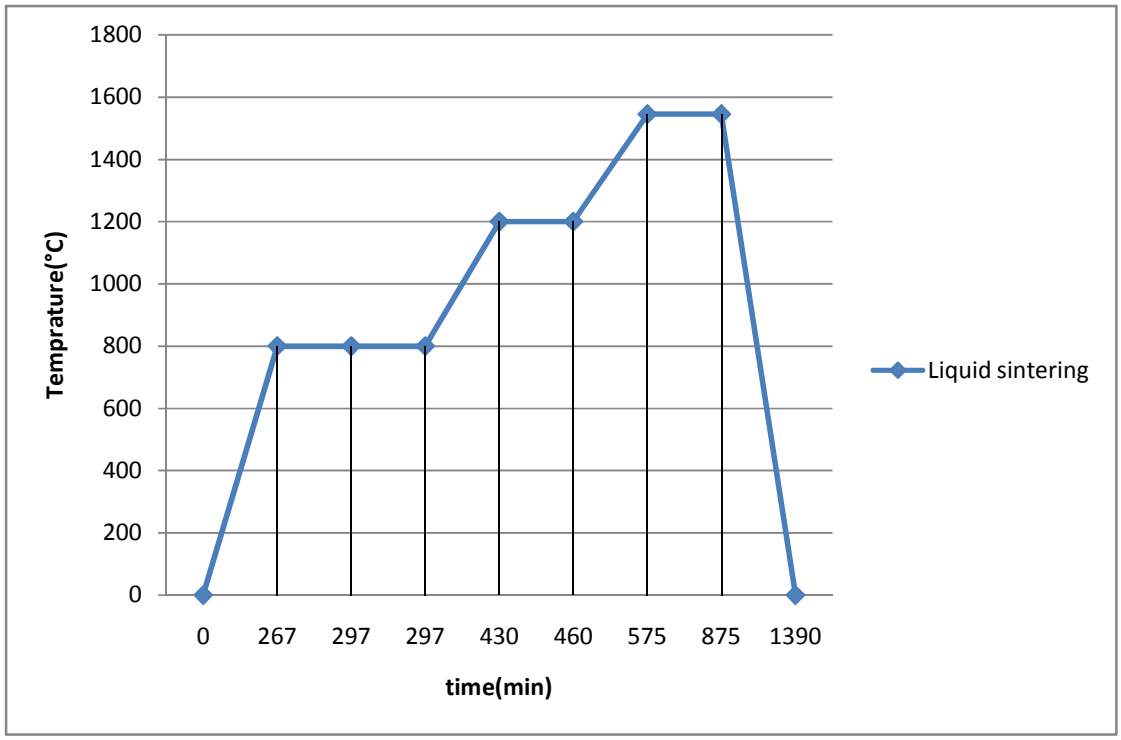

Fig. 4.5 sintering cycle for liquid phase sintering

4.5 Characterization of Sintered Samples

The sintered samples were studied for phase analysis of Al2O3 and CIP, density, VSM, mechanical properties, and micro structural study by optical micro structure and SEM.

- FLOW CHART- In flow chart whole process is shown in systematic manner. In other word flow chart is a mirror image of whole process.

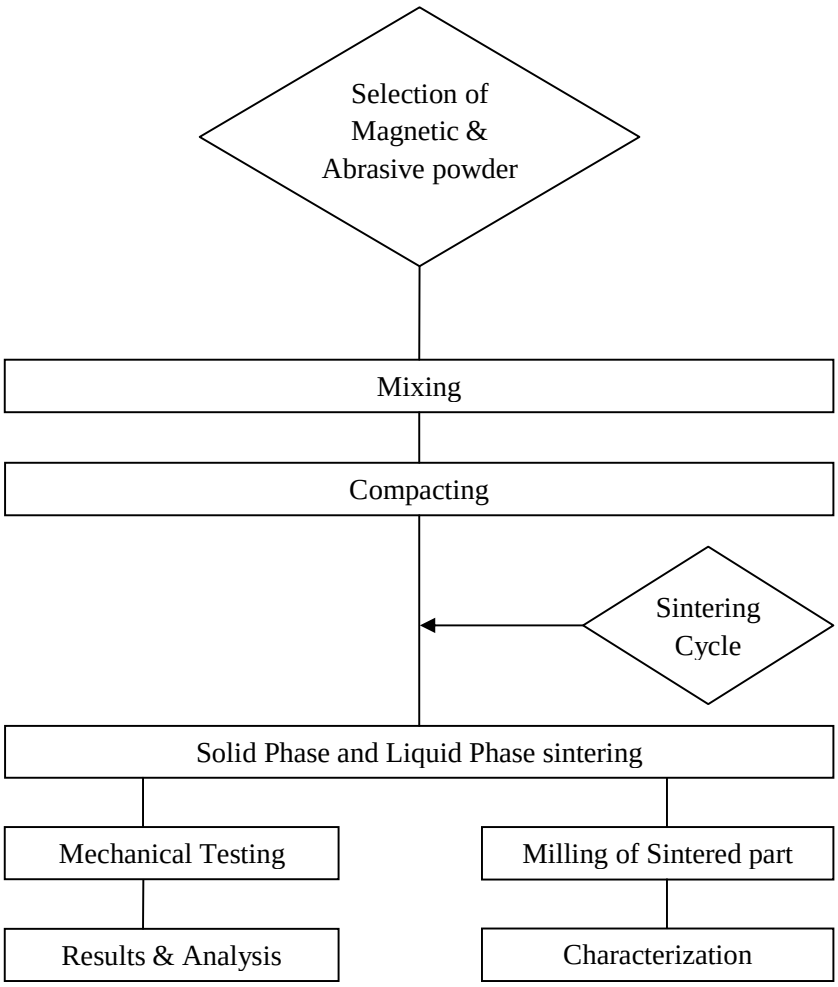

Fig. 4.6 flow chart of process

4.5.1 Micro hardness

The micro hardness was studied by omnitechmmvh auto micro hardness tester. Variation of micro hardness was observed at various points of 5 ton, 7 ton and 9 ton pallets. The hardness of a material is defined as the resistance to indentation. Whereas micro hardness refers to static indentations made with loads not exceeding 1 kgf. The indenter used in this test either the

Vickers diamond pyramid or the Knoop elongated diamond pyramid. The microscopic scale with higher precision instruments is used in this test while rest is similar to standard Vickers hardness test. Precision microscopes (magnification of around X500) are used to measure the indentations. The Knoop hardness number (KHN) is used to calculate it. The Knoop hardness number (KHN) is the ratio of the load applied to the indenter, P (kg f) to the unrecovered projected area A (mm^2).

Where

F= applied load in kgf

A = the unrecovered projected area of the indentation in mm^2

L = measured length of long diagonal of indentation in mm

C = Constant of each indenter supplied by each manufacturer

Sintered parts are prepared by grinding and polishing and leveled by emery paper. Then dry and wet etched for proper surface preparation for making metallographic test specimens.

Fig. 4.7 Omnitechmmvh Auto Micro hardness tester

4.5.2 **Microstructure**

Microstructure was observed by Olympus GX 41 Microscope with META-Lite software. In this microstructure analysis the whole process consists of following steps.

- Dry polishing.
- Wet polishing- In wet polishing alumina powder and water was used.
- Etching- In this process, solution of HNO3+alcohol was used. The purpose of etching to remove thin layer on the surface. Secondly, the etchant attacks the surface with preference for those sites with the highest energy, leading to surface relief which allows different crystal orientation, grain boundaries, and defects to be distinguished in reflected light microscopy.

Olympus GX 41 microscope has magnification range from 25x to 100x.

Fig.4.8 Olympus GX 41microscope

4.5.3 UNIVERSAL TESTING MACHINE

Compressive strength was observed by universal testing machine. Compressive stress is easily calculated by the value of compressive strength. As we know that,

Compressive stress = load/area

Here radius of pallet =6.5 mm

Fig. 4.9 Universal Testing Machine

4.5.4 X-ray diffraction

The phase analysis of powder was carried out with an X-ray diffractometer (Bruker AXS D8 Advance instrument) with Cu-Kα radiation in the 2θ range 5-110° at a scan speed of 2°/min. and also identified crystalline peaks. FWHM value was observed.

Fig. 4.10 X-ray diffractometer (Bruker AXS D8 Advance instrument)

4.5.5 SEM ANALYSIS

Microstructure and morphological characteristics of coatings were obtained by SEM and with the help of Energy Dispersive Spectroscopy (EDS) calculate the % composition of metal and ceramic in Alumina and CIP composite coatings. EDS shown the peaks of maximum energy where most X-rays have been received.

Fig. 4.11 Scanning Electron Microscopy (SEM)

4.5.6 VSM ANALYSIS

Magnetic Moment was done by Vibrating Sample Magnetometer. Max current 30 amp. , weight of the sample 0.7485 gm, scan time 900 sec. VSM range 10 , gauss meter range 10 were used .

Fig. 5.12 Vibrating Sample Magnetometer

CHAPTER V

RESULT AND DISCUSSIONS

5.1 DENSITY

Bulk density increase with compaction load of sintered pallets because when compaction load increase then volume of pallets will be decrease and also density of sintered pallets is higher than green pallets because of shrinkage of volume of pallets.

Sample No-	sample	Density(gm/cc3)	
		Green sample	Sintered sample
1	5 ton solid	3.05	3.3
2	7 ton solid	3.1	3.32
3	9 ton solid	3.3	3.4
4	7 ton liquid	3.1	3.45
5	9 ton liquid	3.3	3.49

Table 5.1- density of green pallets vs. sintered pallets

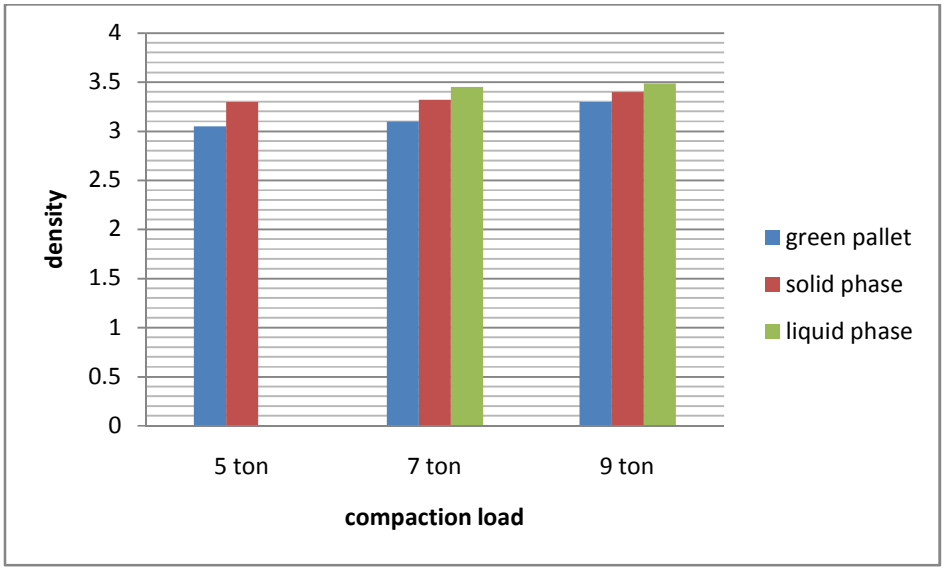

Fig 5.1 Density graph of green pallets vs. sintered pallets

5.2 Micro hardness

The micro hardness values were calculated at various points of pallets. The data obtained showed that the 9 ton pallet has maximum hardness value. The micro hardness values increase with compaction load. Hardness is the resistance offered by the crystal for the movement of dislocations and practically it is the resistance offered by the crystal for localized plastic deformation. Hence from result it is clear that resistance offered by the crystal increase with higher compaction load.

SAMPLE NO.-	SAMPLE	MCROHARDNESS(VHN)
1	5 ton solid	430
2	7 ton solid	490
3	9 ton solid	517
4	7 ton liquid	530
5	9 ton liquid	650

Table 5.2- Micro hardness no. of sintered pallets

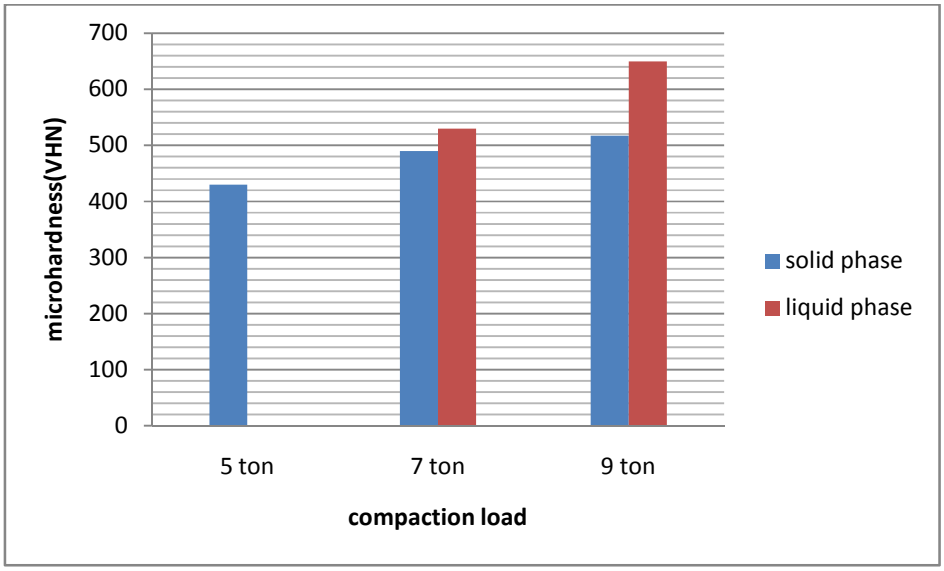

Fig 5.2 Micro hardness (VHN) graph of sintered pallets

5.3 compressive Stress

Compressive stress increases with compaction load of pallets and has higher value in the case of liquid phase sintering. Hence compressive stress depends on load and temperature.

Sample no-	sample	Compressive stress (N/mm2)
1	5 ton solid	43.56
2	7 ton solid	57.13
3	9 ton solid	75.33
4	7 ton liqud	57.72
5	9 ton liquid	67.95

Table 5.3 compressive stress observation with compaction load

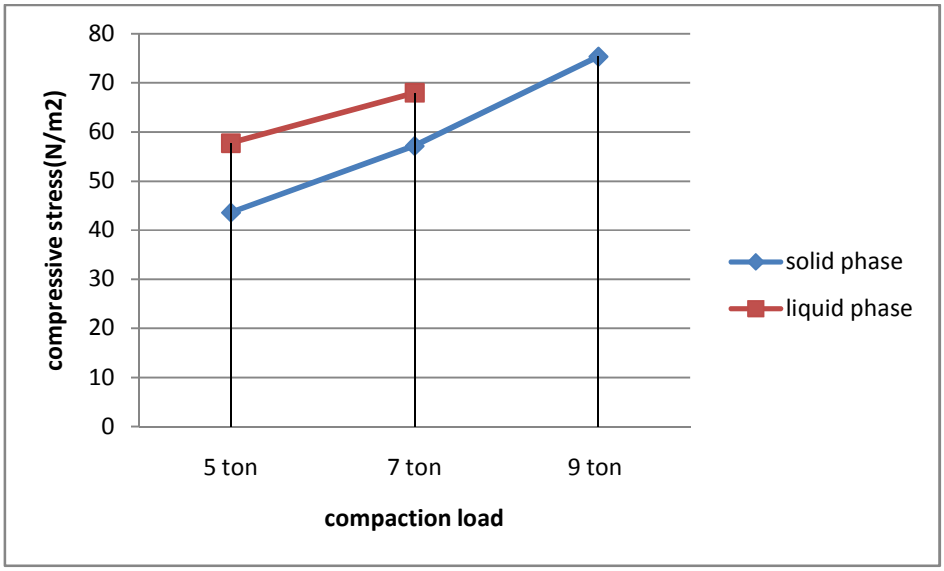

Fig.5.3 compaction load vs. compaction stress

5.4 Micro structure Analysis

Micro structure analysis was observed by optical microscope with 100x magnification of 5 ton solid , 7 ton solid, 9ton solid, 7 ton liquid and 9 ton liquid. From fig. (**5.9-5.11**) it is clear that there are two phase present in the sample. In the coloured part green portion is alumina and the red portion is iron. **Fig. 5.4-5.8** shows microstructure of samples and results are all white portion is alumna and black spot is iron.

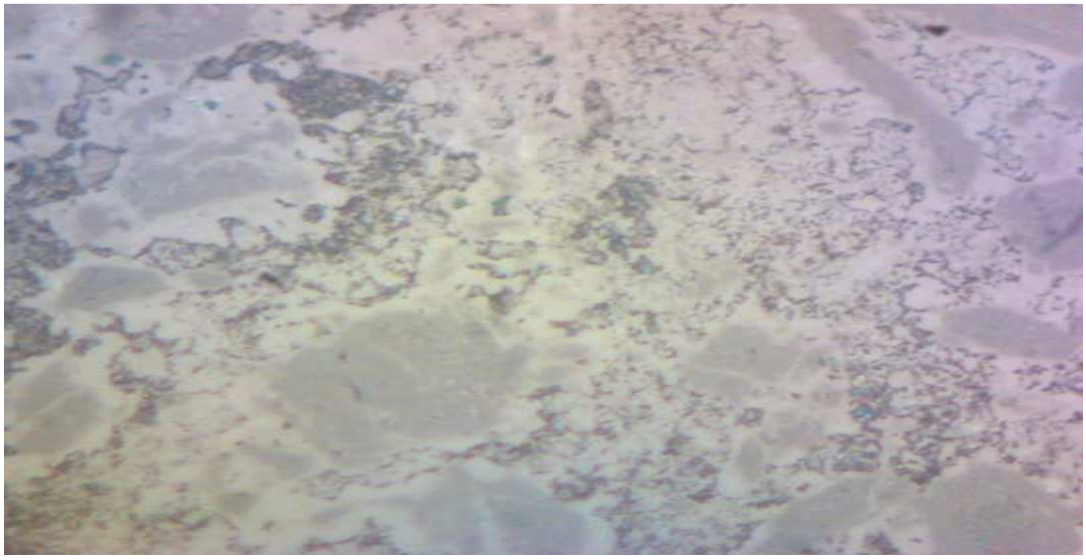

Fig 5.4 micro structure of 5 ton solid phase

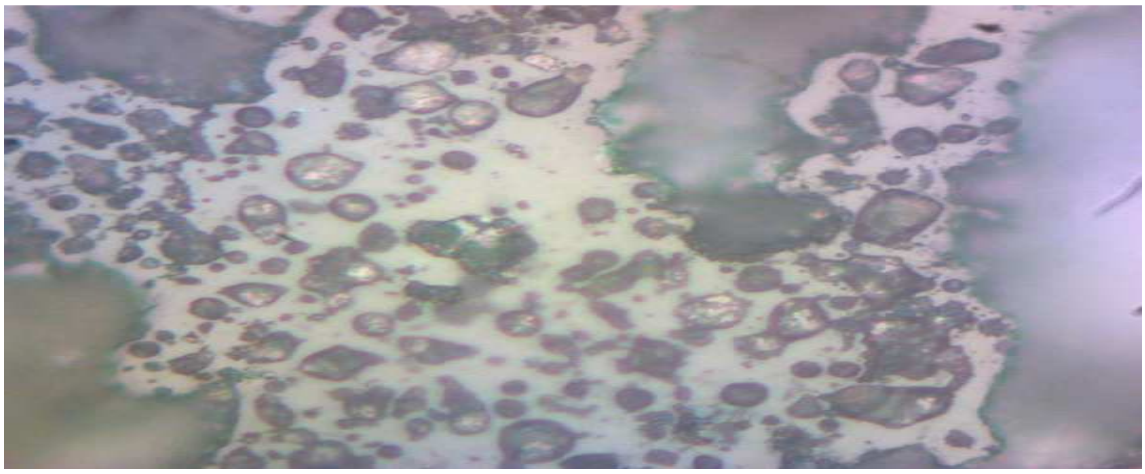

Fig 5.5 micro structure of 7 ton solid phase

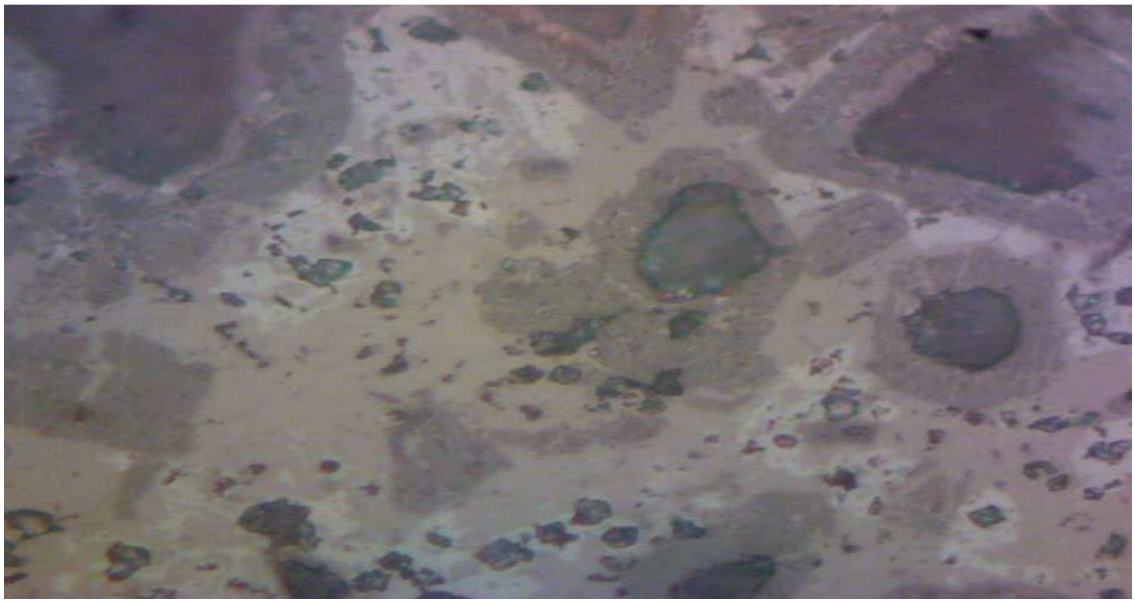

Fig 5.6 micro structure of 9 ton solid phase

Fig 5.7 micro structure of 7 ton liquid phase

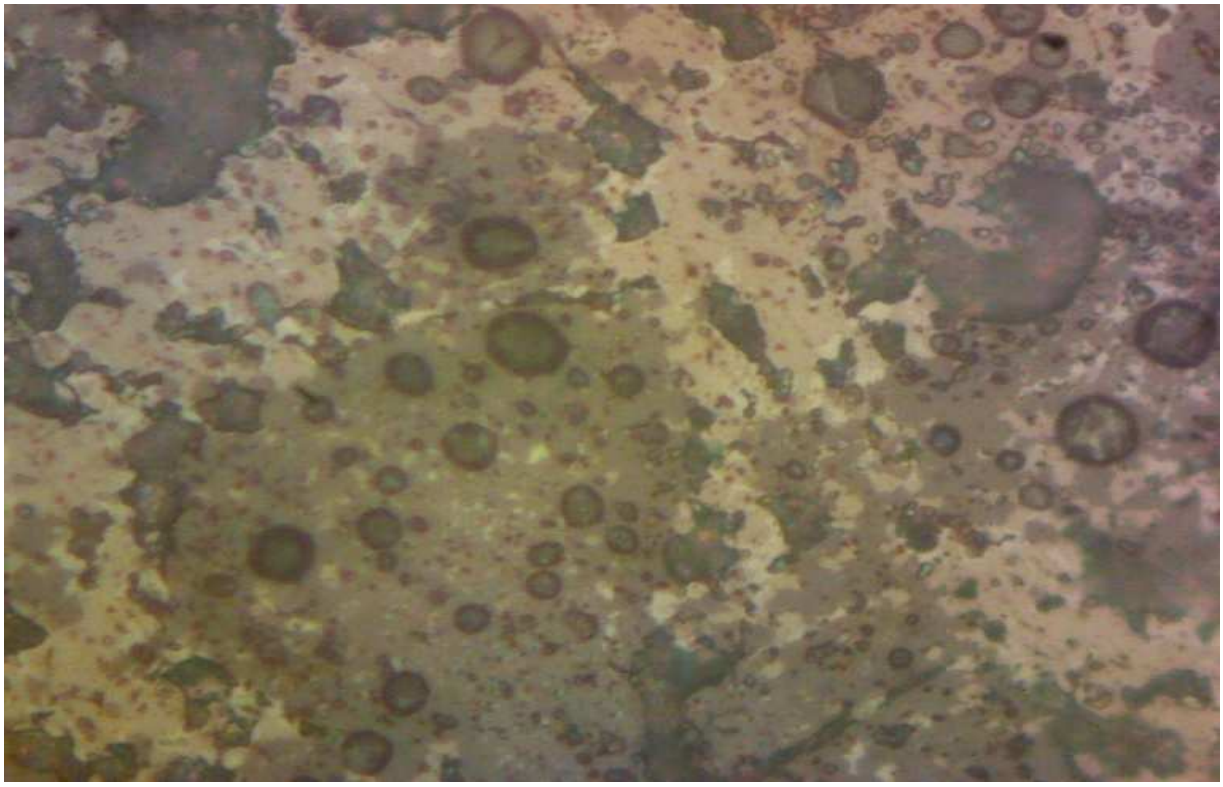

Fig 5.8 micro structure of 9 ton liquid phase

CUSTOMER	Adam	**MATERIAL**	Enter Material Name
DATE	9/5/2013	**DESCRIPTION**	Description
HEATNO	9 ton solid	**GRADE**	Grade

MICROSTRUCTURE TEST REPORT

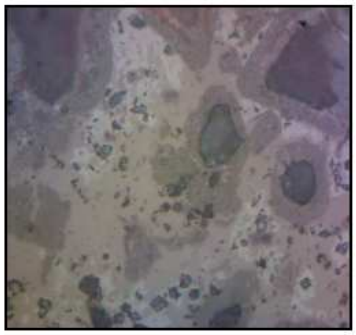

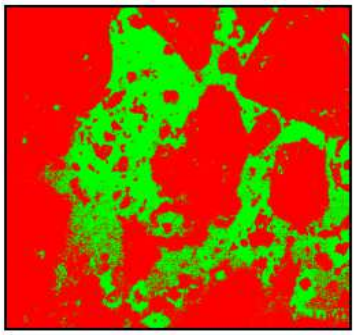

PHASE AND VOLUME ANALYSIS ASTM E562 &E1245

SNo	NAME	AREA	AREA_PER
1	Phase 1	26837.377 Micron Sqr	71.258
2	Phase 2	10825.042 Micron Sqr	28.742

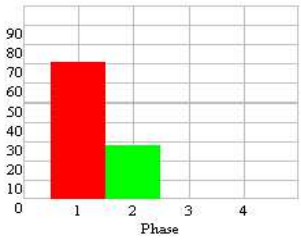

Remarks :

Approved By :

Fig 5.9 micro struture test result of 9 ton solid phase sintering

CUSTOMER	Adam	MATERIAL	al2o3+CIP
DATE	10/4/2013	DESCRIPTION	Description
HEATNO	70ton li	GRADE	Grade

MICROSTRUCTURE TEST REPORT

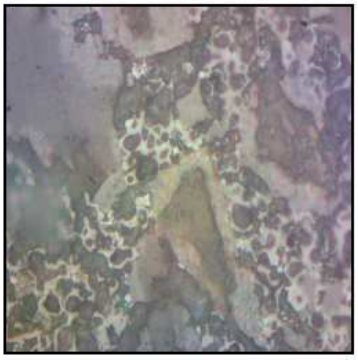

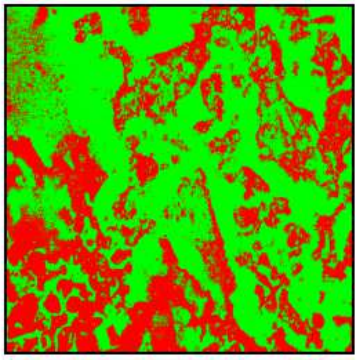

PHASE AND VOLUME ANALYSIS ASTM E562 &E1245

SNo	NAME	AREA	AREA_PER
1	Phase 1	337495.950 Micron Sqr	37.977
2	Phase 2	551187.225 Micron Sqr	62.023

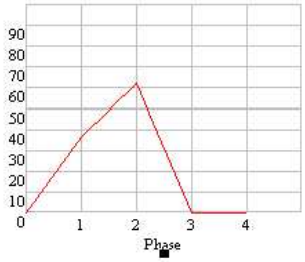

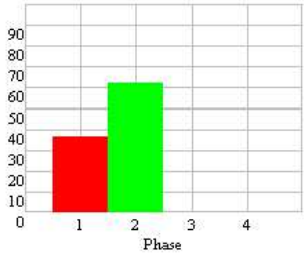

Remarks :

Approved By :

Fig 5.10 micro struture test result of 7 ton liquid phase sintering

CUSTOMER	Adam	**MATERIAL**	Enter Material Name
DATE	10/4/2013	**DESCRIPTION**	Description
HEATNO	9ton li	**GRADE**	Grade

MICROSTRUCTURE TEST REPORT

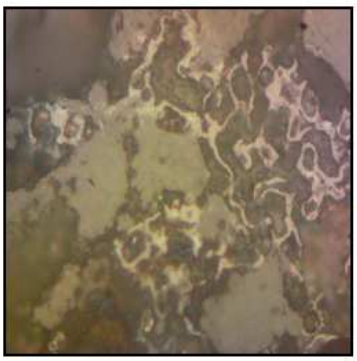

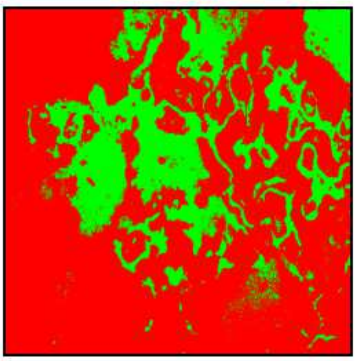

PHASE AND VOLUME ANALYSIS ASTM E562 &E1245

SNo	NAME	AREA	AREA_PER
1	Phase 1	660200.879 Micron Sqr	74.29
2	Phase 2	228482.296 Micron Sqr	25.71

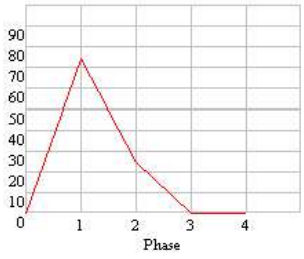

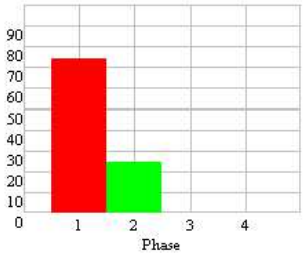

Remarks :

Approved By :

Fig 5.11 micro struture test result of 9 ton liquid phase sintering

5.5 SEM ANALYSIS

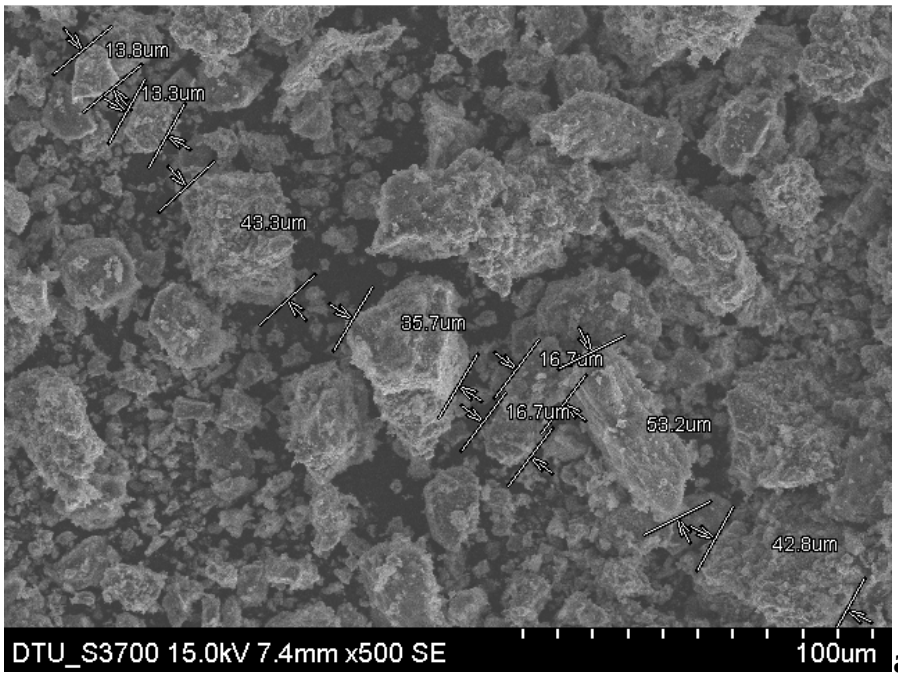

a

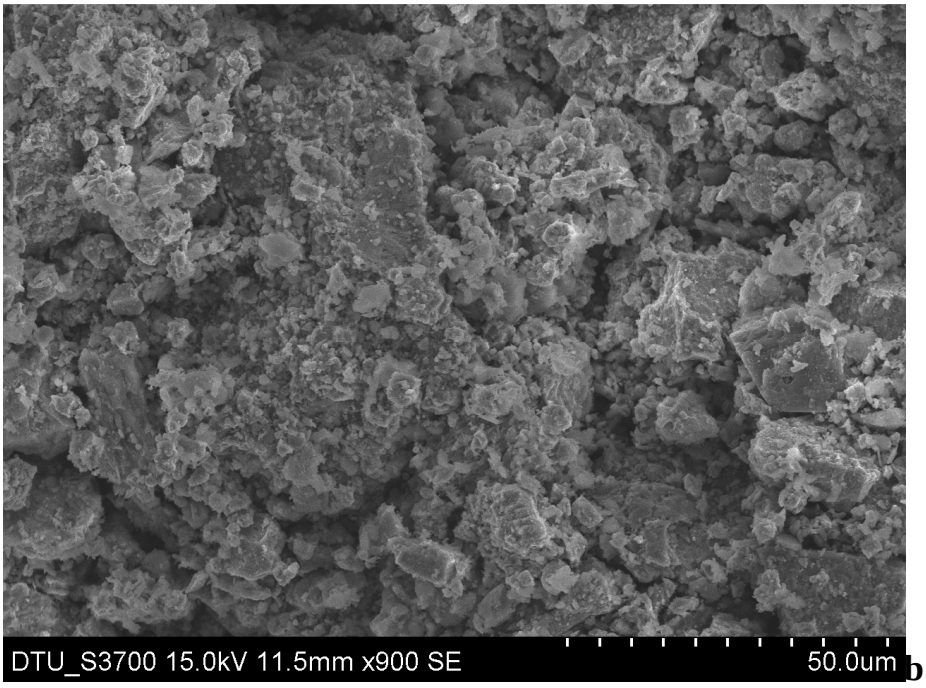

b

Fig 5.12 SEM micro graph of 5 ton solid sintered sample

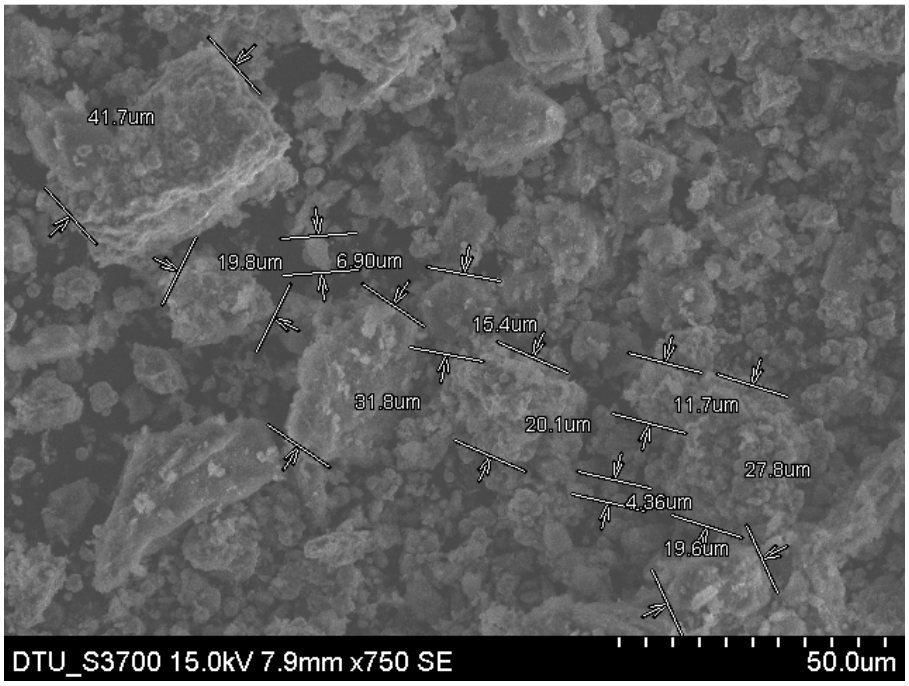

a

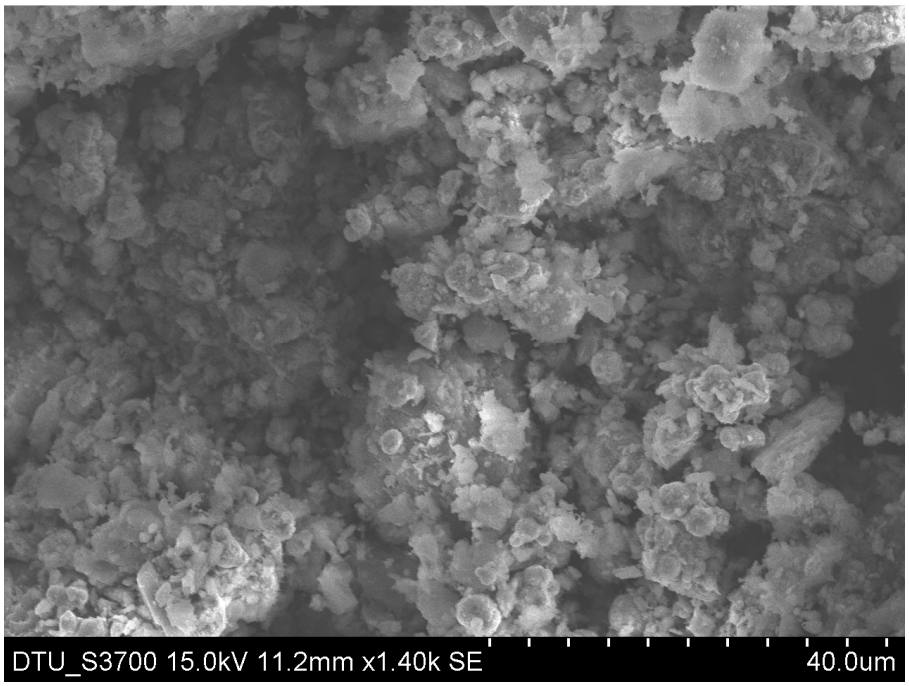

b

Fig 5.13 SEM micro graph of 7 ton solid sintered sample

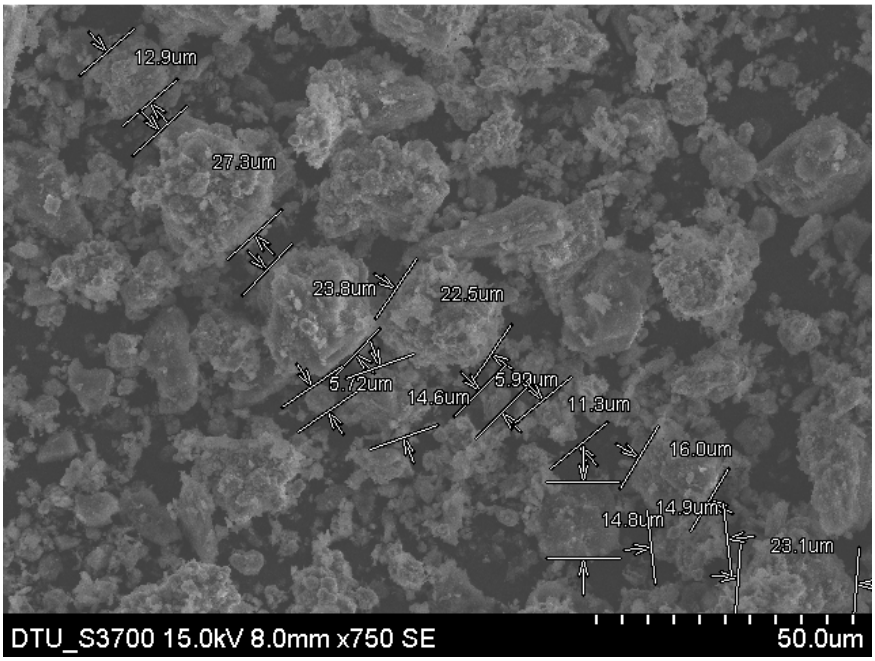

a

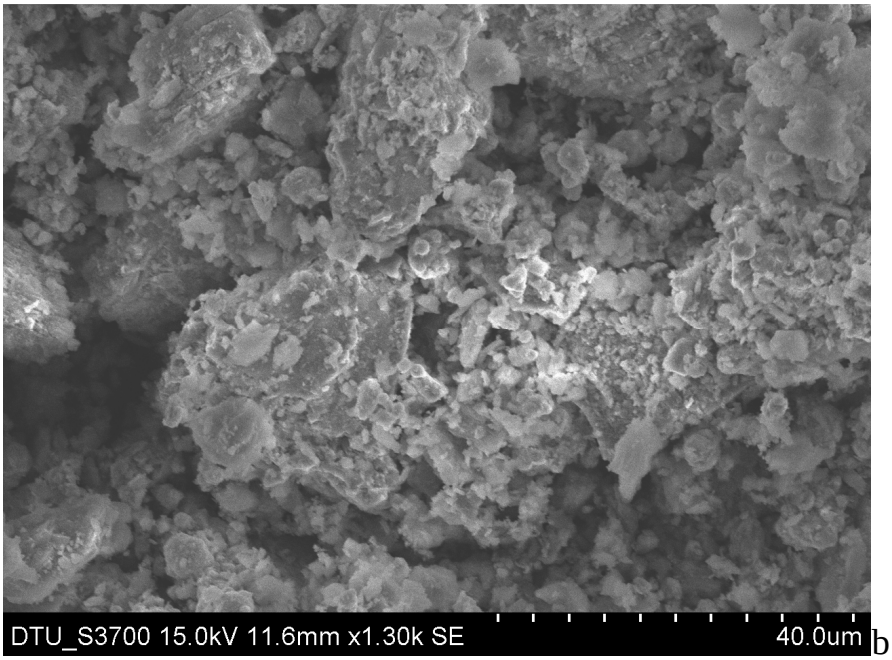

b

Fig 5.14 SEM microstructure of 9 ton solid sintered sample

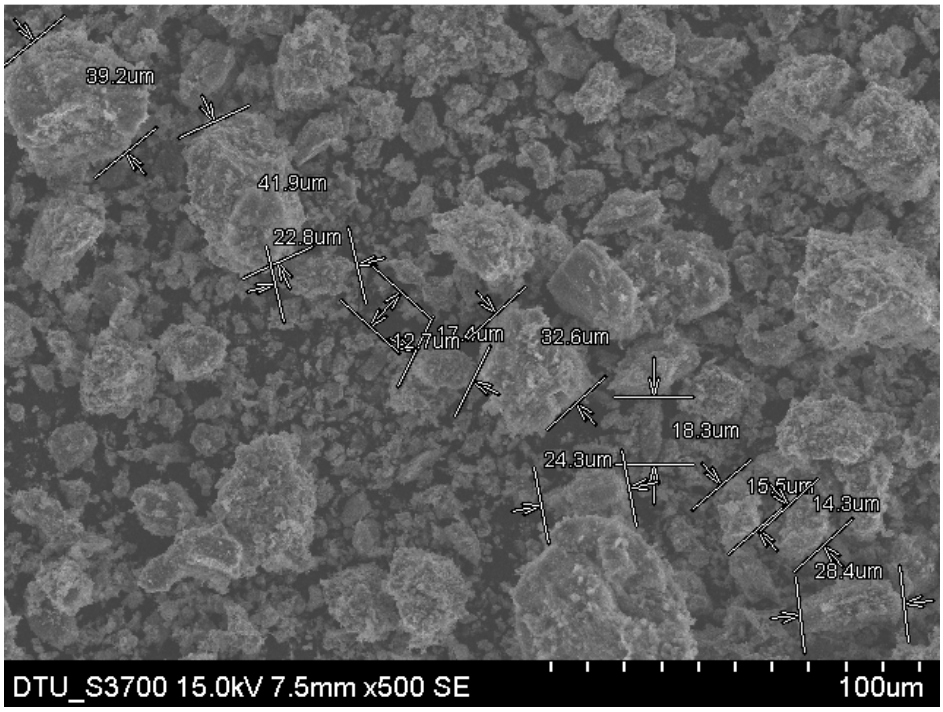

a

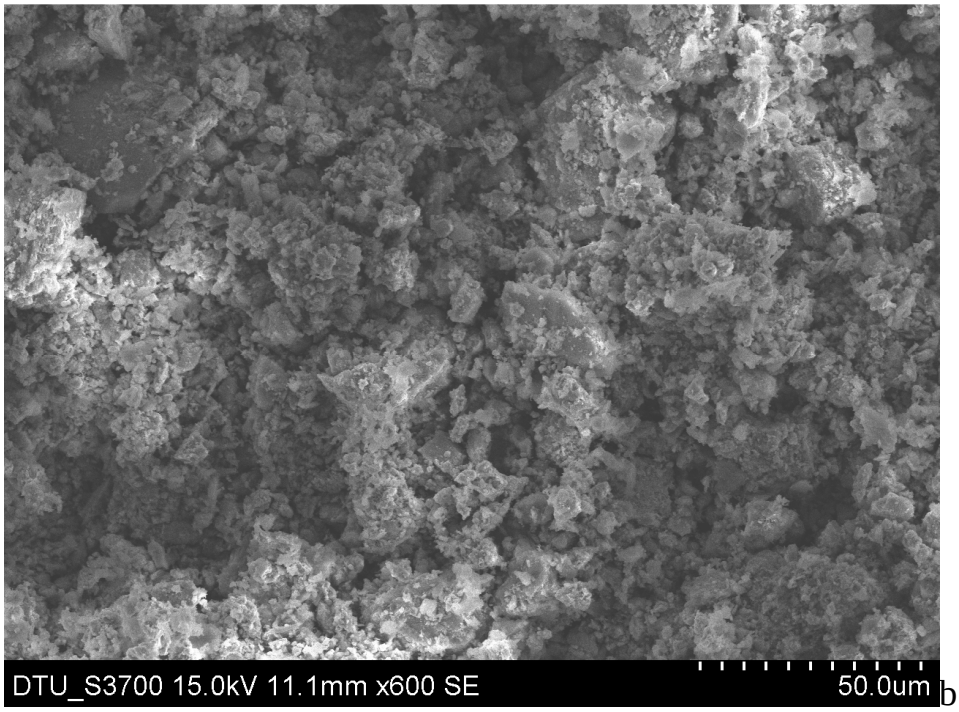

b

Fig.5.15 SEM microstructure of 7 ton liquid sintered sample

Figure (5.12-5.15) shows SEM micro graph for sintered sample. In each figure (a) gives diagonally particle size. In sample 5ton solid the average particle size respect to diagonal is 29μ_m , the diagonally average particle size of 7 ton liquid is 19.9μ_m, for 9 ton solid its value is 14.09μ_m and for 7 ton liquid average particle size is 24.03μ_m. In each figure (b), Sharpe edge particle is alumina and iron particle diffused on it.

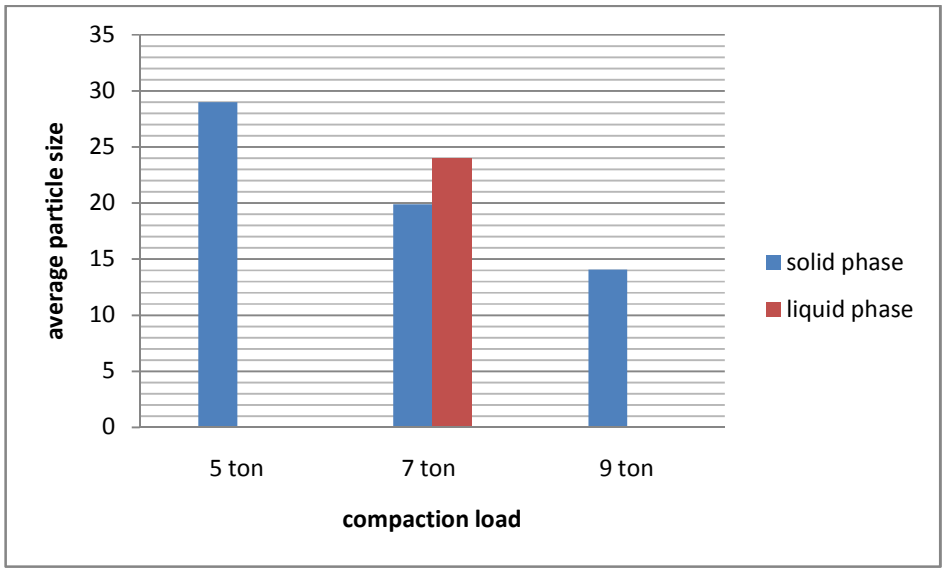

Fig 5.16 graph of average particle size vs. compaction load

5.6 EDX ANALYSIS

EDX analysis of the composites to confirm the existence of iron, carbon , oxygen, and alumina. For EDX purpose accelerated Voltage was used 15.0 KV and take off angle 54.6 degree.

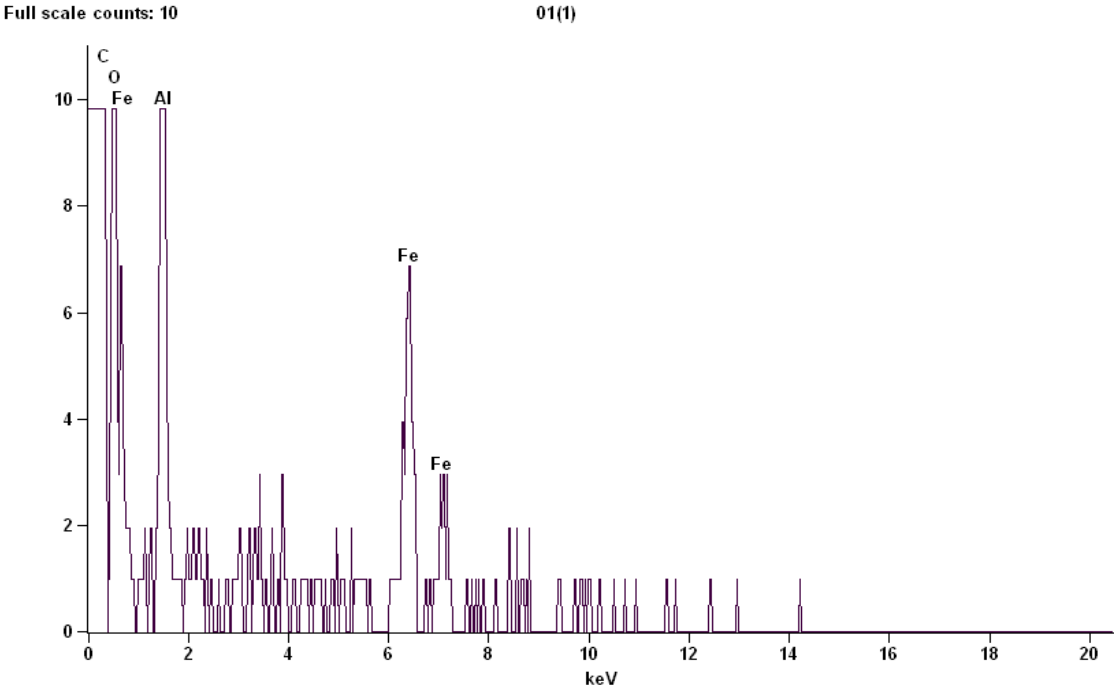

Fig 5.17 EDX graph of 5 ton solid

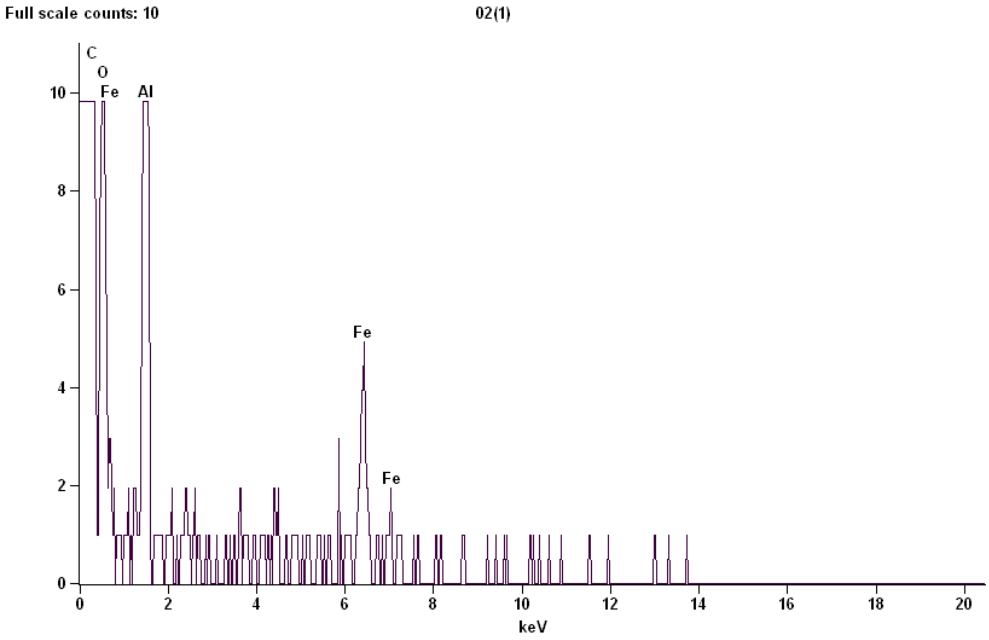

Fig 5.18 EDX graph of 7 ton solid

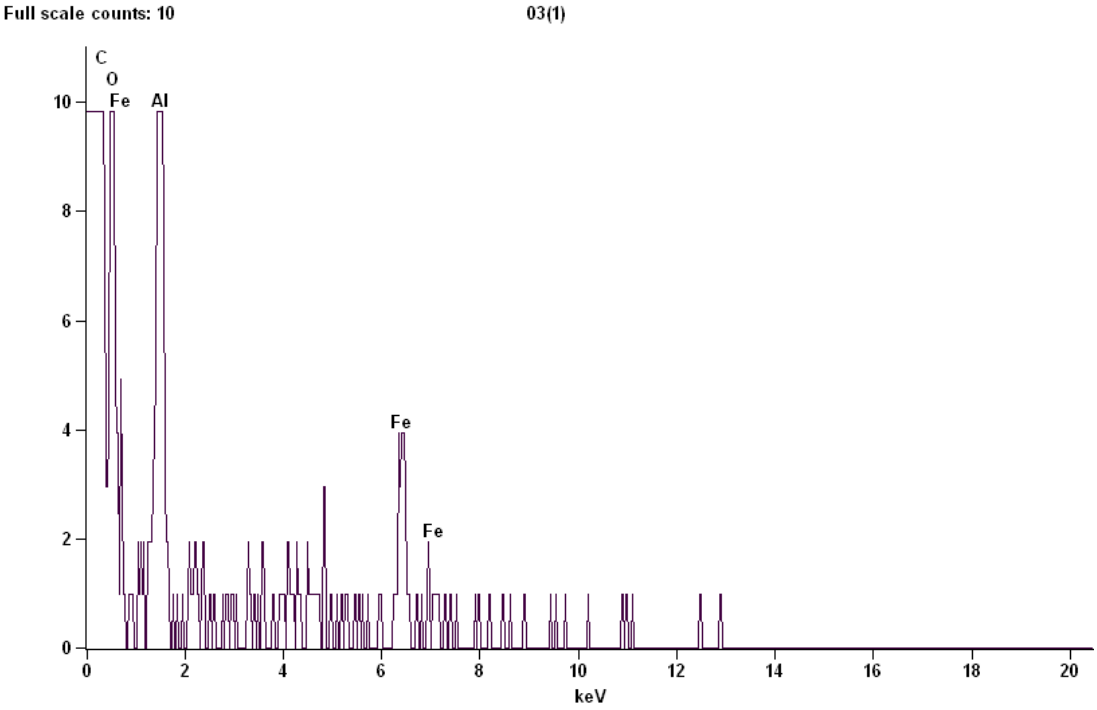

Fig 5.19 EDX graph of 7 ton liquid

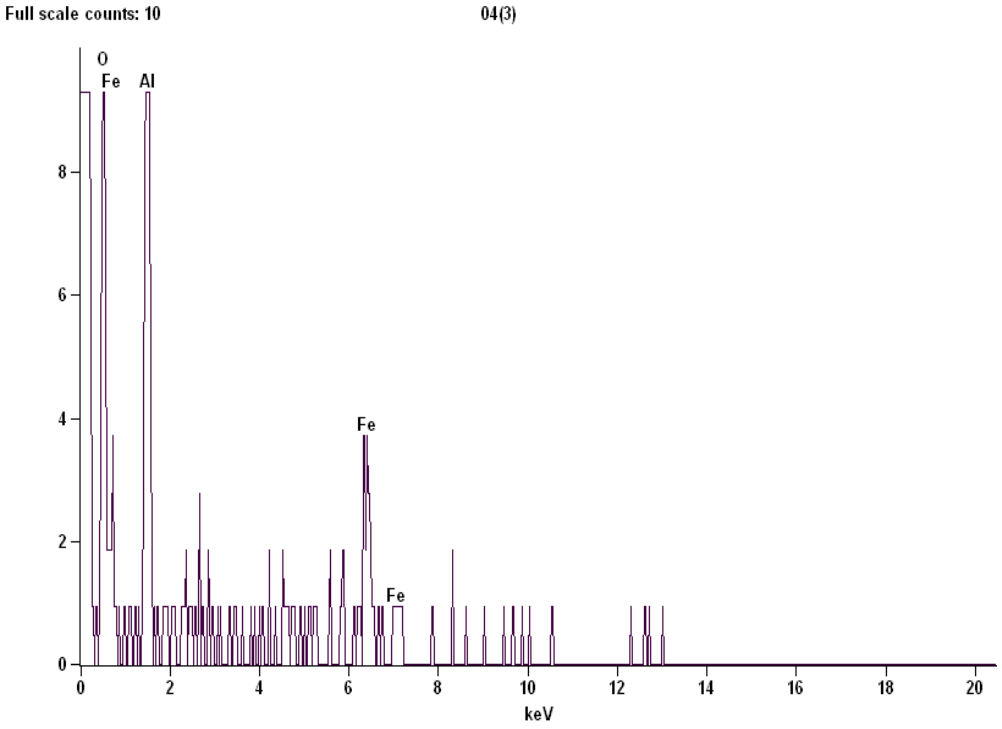

Fig 5.20 EDX graph of 7 ton liquid

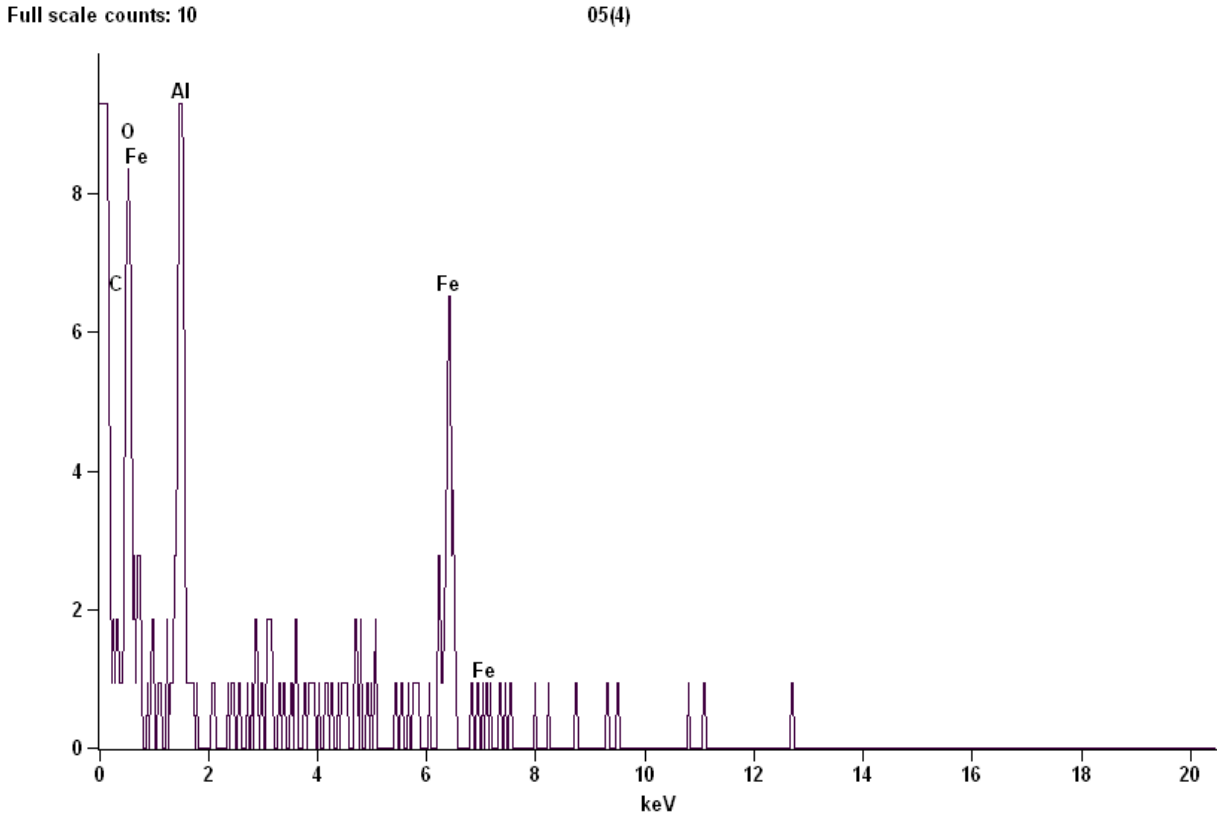

Fig 5.21 EDX graph of 9 ton liquid

5.7 Phase evolution of sintered sample

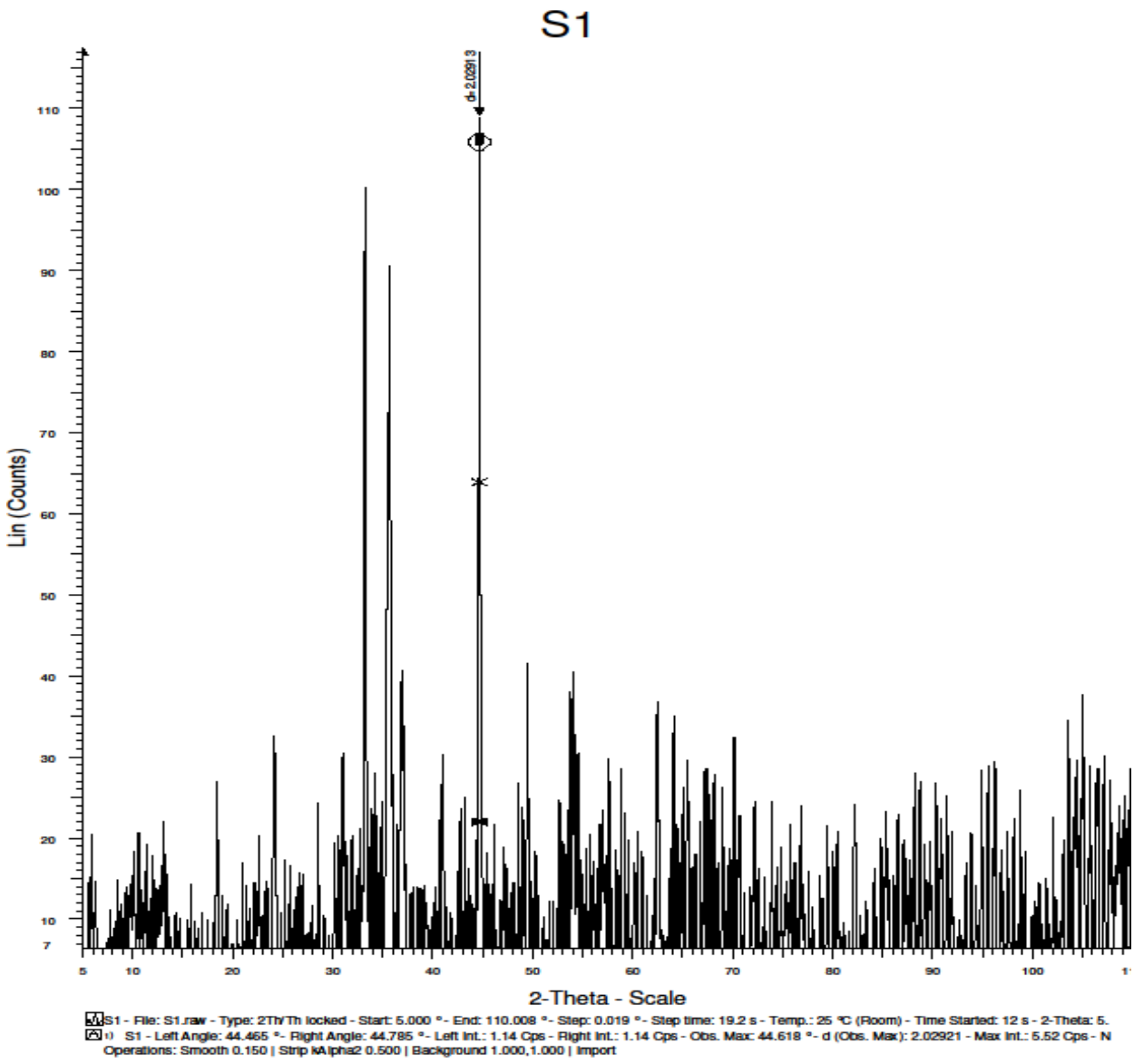

Fig.5.22 XRD pattern for 5 ton solid sample.

The XRD pattern of 5 ton solid sintered alumina and CIP is shown in fig. 5.22 and fig. 5.23. From these figure first peak comes at 33.180°. This peaks belongs to Fe_2o_3 and has (1, 0, 4) h, k, l value, his plane is simple cubic. Second phase is at 33.280° of Al_2o_3 has (1, 0, 4) h k l value and his plane is simple cubic. Third peaks is at 35.452 of Fe_3o_4 has (3, 1, 1) h k l values and his plane is Fcc. Fourth pick is at 44.142° of Fe has (1, 1, 0) h k l value and his plane is Bcc. Fifth peak is at 54.233° of Fe_2o_3 has (1, 1, 6) and his plane is simple cubic. For this sample FWHM value of highest peak is 016°.

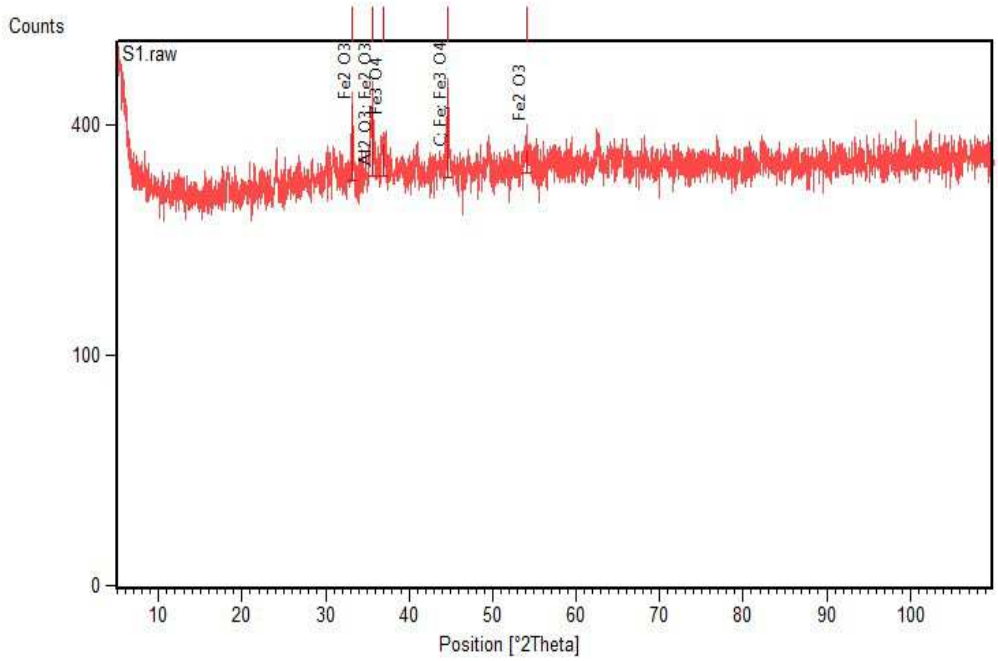

Fig.5.23 XRD pattern for peak composition of 5 ton solid sample

The XRD pattern of sintered alumina and CIP is shown in fig. 5.24 and fig. 5.25. From these figure first peak comes at 33.180°. This peaks belongs to Fe_2o_3 and has (1, 0, 4) h, k, l value, his plane is simple cubic. Second phase is at 33.280° of Al_2o_3 has (1, 0, 4) h k l value and his plane is simple cubic. Third peaks is at 35.452 of Fe_3o_4 has (3, 1, 1) h k l values and his plane is Fcc. Fourth pick is at 44.142° of Fe has (1, 1, 0) h k l value and his plane is Bcc. Fifth peak is at 54.233° of Fe_2o_3 has (1, 1, 6) and his plane is simple cubic. Sixth peak is at 65.686°of Fe has (2, 0,0) and his planes is Bcc. The FWHM value for highest peak is 0.127°.

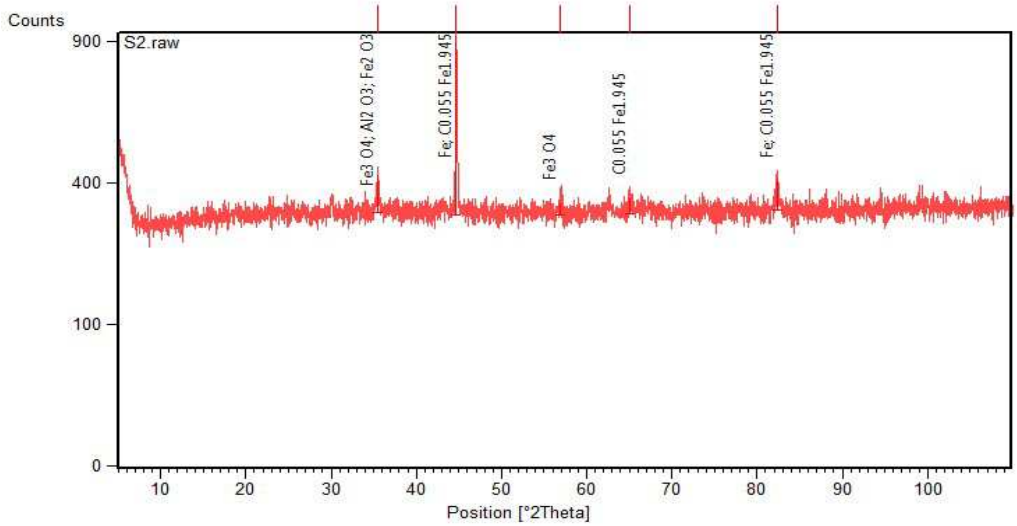

Fig 5.24 XRD pattern for peak composition of 7 ton solid sample

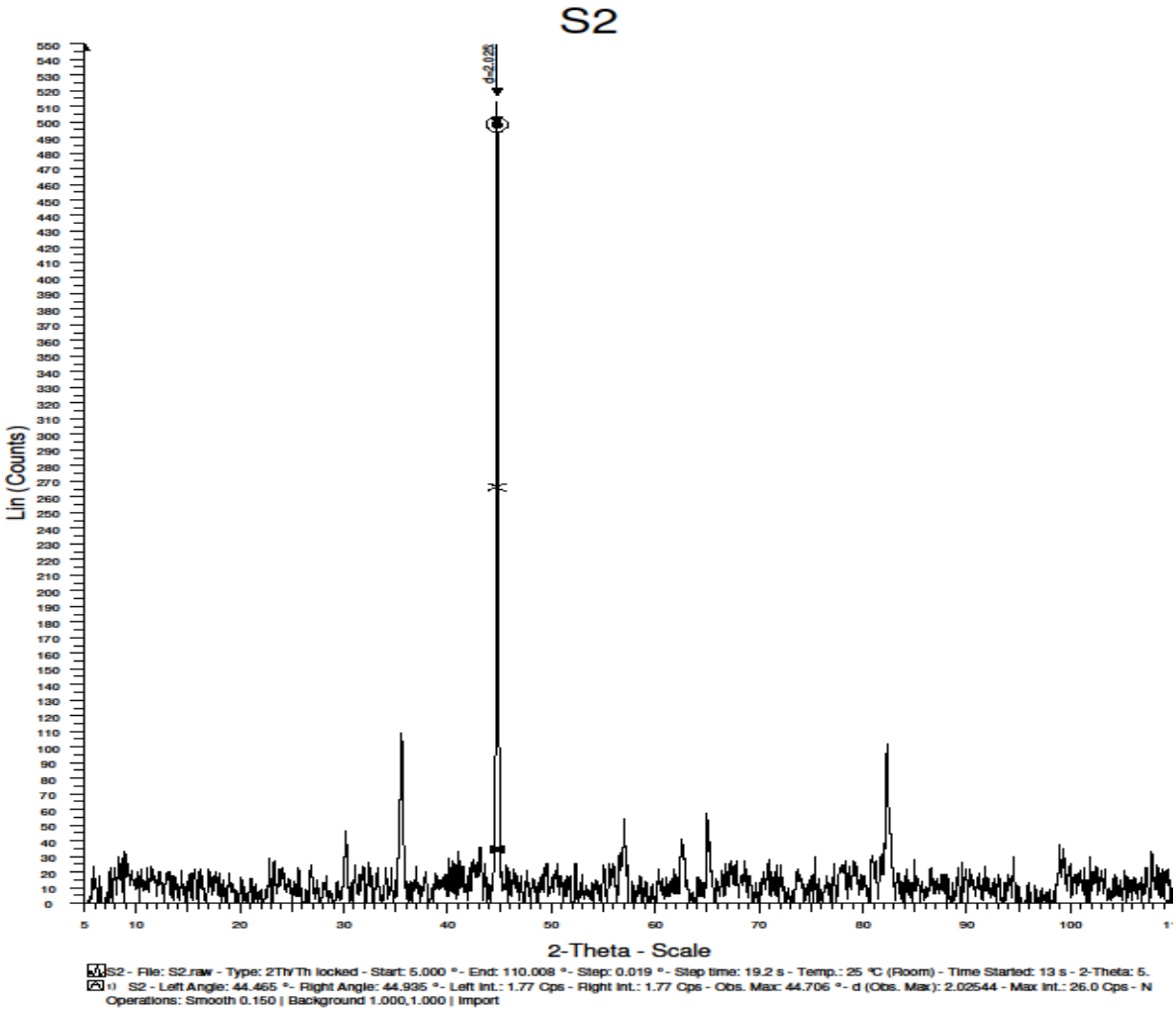

Fig.5.25 XRD pattern for 7 ton solid sample

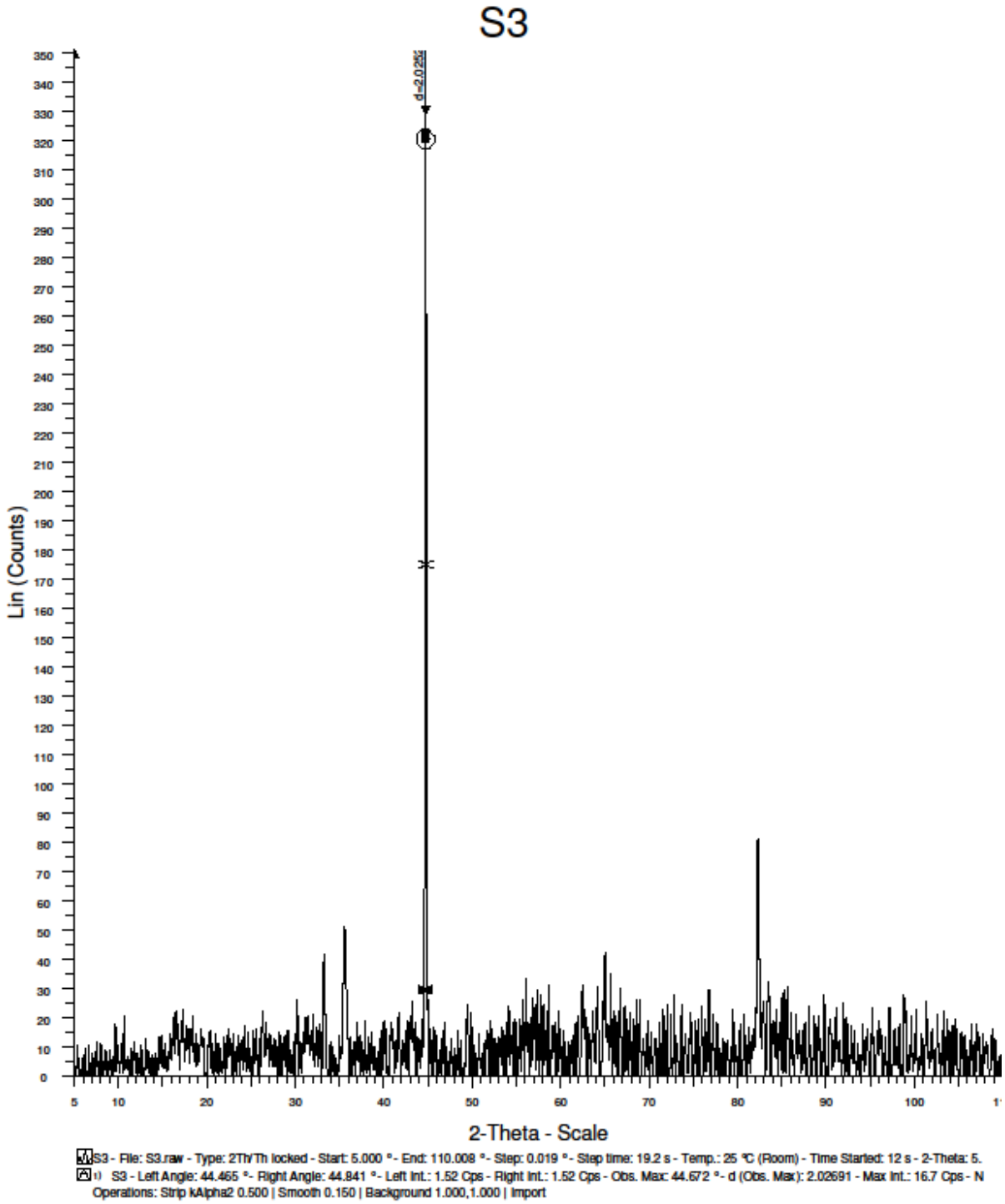

Fig.5.26 XRD pattern for 9 ton solid sample.

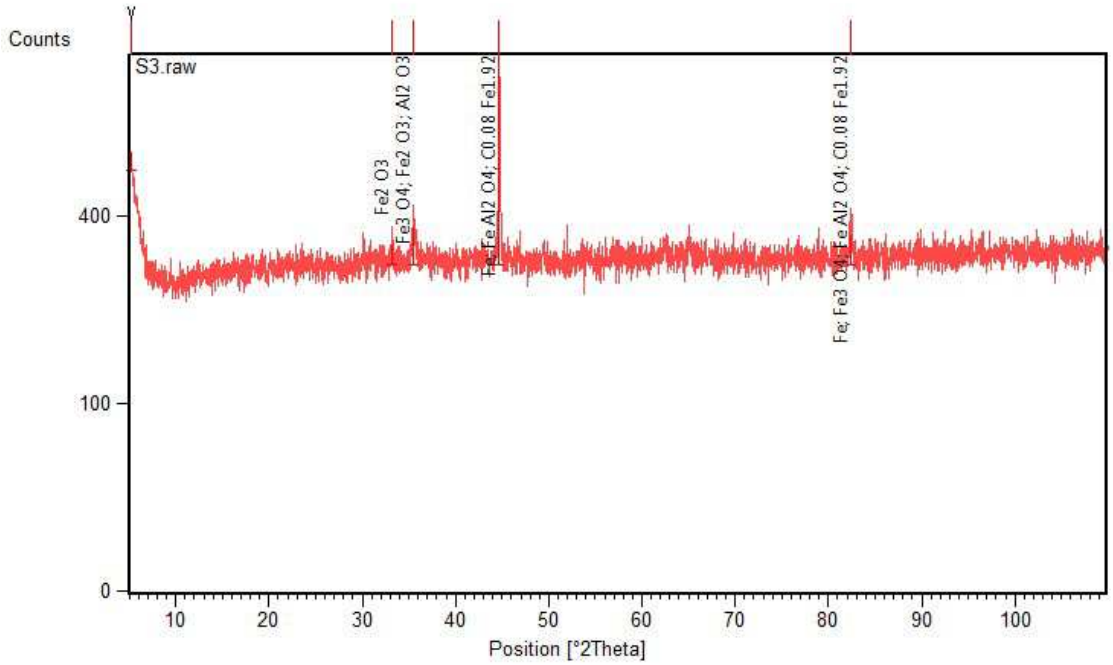

Fig.5.27 XRD pattern for peak composition of 9 ton solid sample

The XRD pattern of sintered alumina and CIP is shown in fig. 5.26 and fig. 5.27. From these figure first peak comes at 33.180°. This peaks belongs to Fe_2o_3 and has (1, 0,4) h ,k, l value , his plane is simple cubic. Second phase is at 33.280° of Al_2o_3 has (1, 0, 4) h k l value and his plane is simple cubic. Third peaks is at 35.452 of Fe_3o_4 has (3, 1, 1) h k l values and his plane is Fcc. Fourth pick is at 44.142° of Fe has (1, 1, 0) h k l value and his plane is Bcc. Fifth peak is at 83.219° of Fe has (2, 1, 1) and his plane is Bcc.. The FWHM value for highest peak is 0.188°.

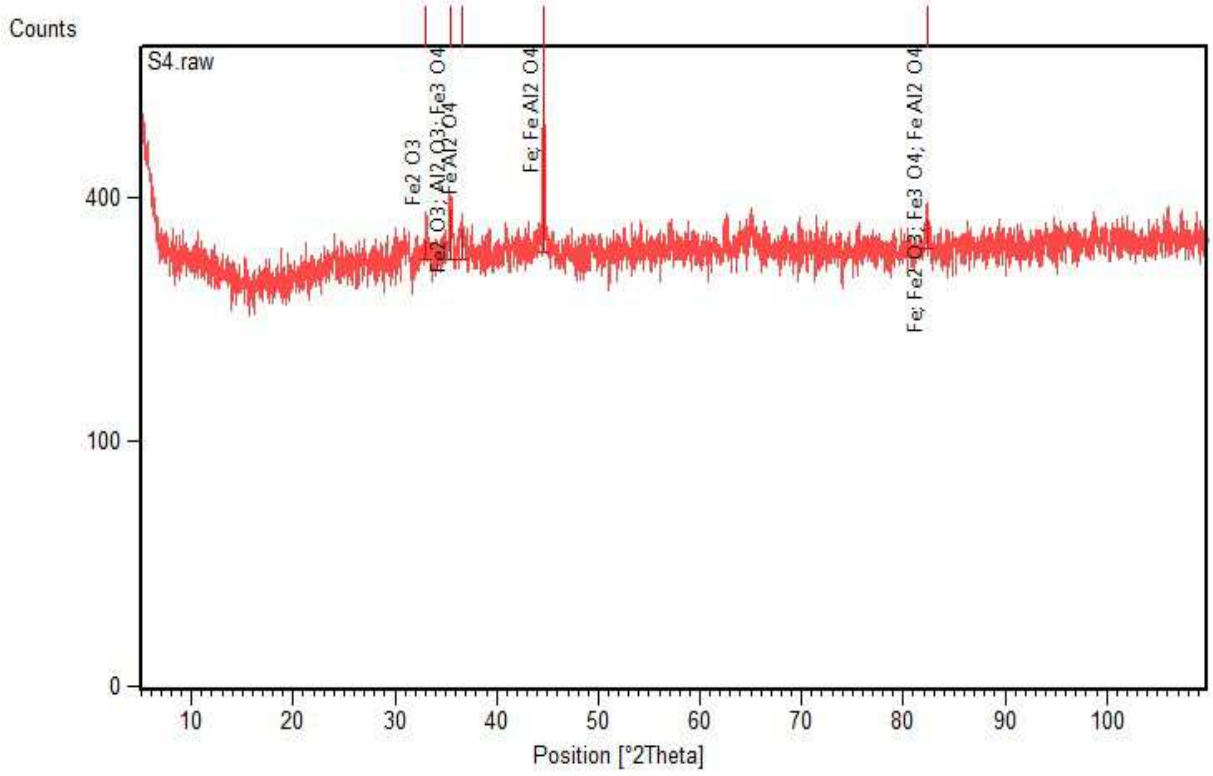

Fig.5.28 XRD pattern for peak composition of 7 ton liquid sample

The XRD pattern of sintered alumina and CIP is shown in fig. 5.28 and fig. 5.29. From these figure first peak comes at 33.180°. This peaks belongs to Fe_2o_3 and has (1, 0,4) h ,k, l value , his plane is simple cubic. Second phase is at 33.280° of Al_2o_3 has (1, 0, 4) h k l value and his plane is simple cubic. Third peaks is at 35.452 of Fe_3o_4 has (3, 1, 1) h k l values and his plane is Fcc. Fourth pick is at 44.142° of Fe has (1, 1, 0) h k l value and his plane is Bcc. Fifth peak is at 83.219° of Fe has (2, 1, 1) and his plane is Bcc.. The FWHM value for highest peak is 0.174°.

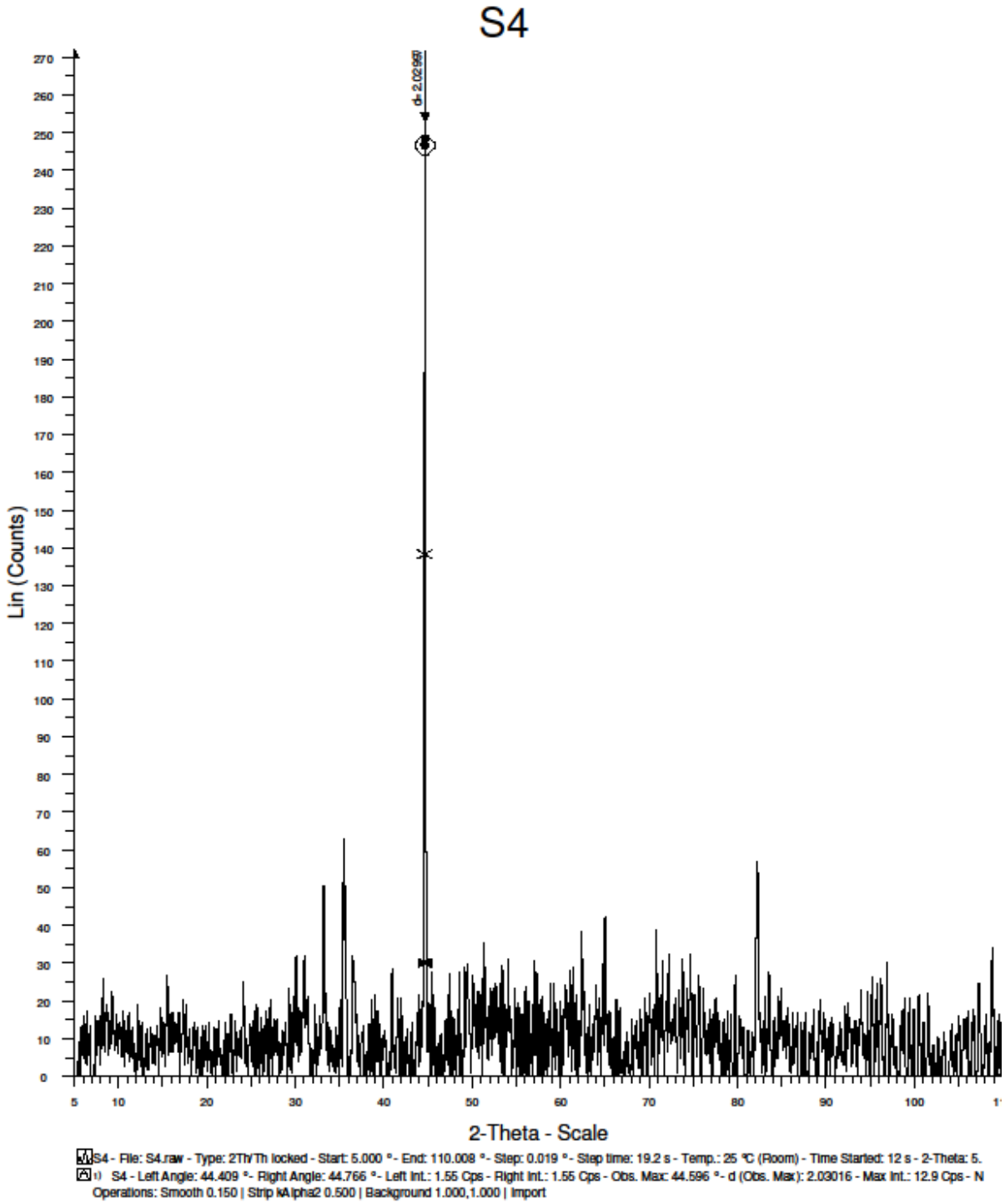

Fig 5.29 XRD pattern for 7 ton liquid sample.

5.8 VSM ANALYSIS.

VSM shows magnetic strength of sample. When a ferromagnetic material is magnetized in one direction, it will not relax back to zero magnetization when the imposed magnetizing field is removed. It must be driven back to zero by a field in the opposite direction. From the value of magnetic moment it is clear that the value of magnetic moment increase with compaction load and sintering temperature.

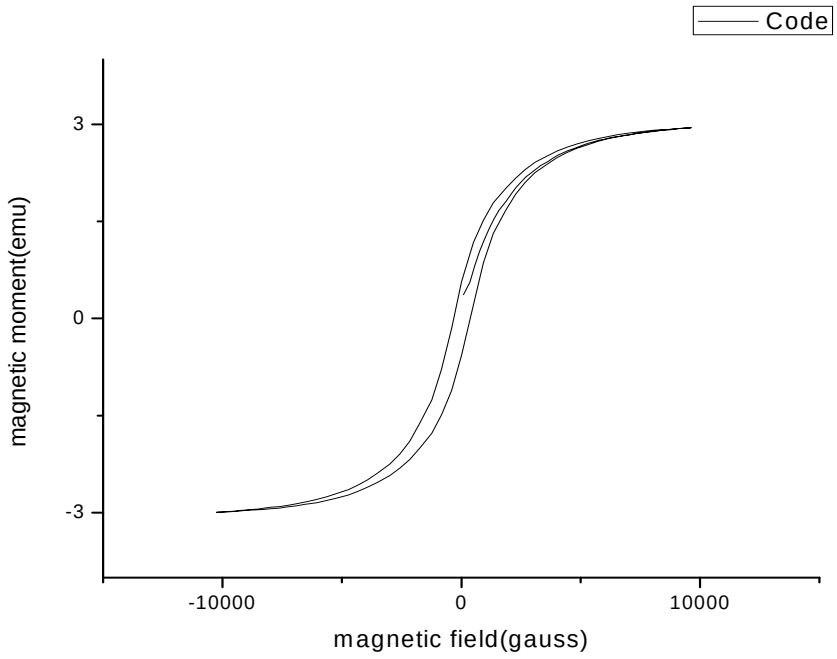

Fig.5.30 Graph between magnetic moment vs. magnetic field of 5 ton solid

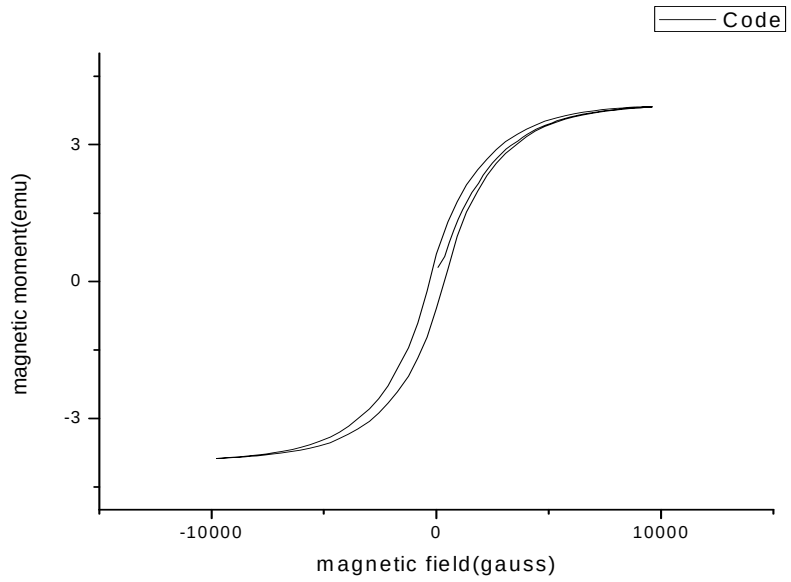

Fig. 5.31Graph between magnetic moment vs. magnetic field of 7 ton solid

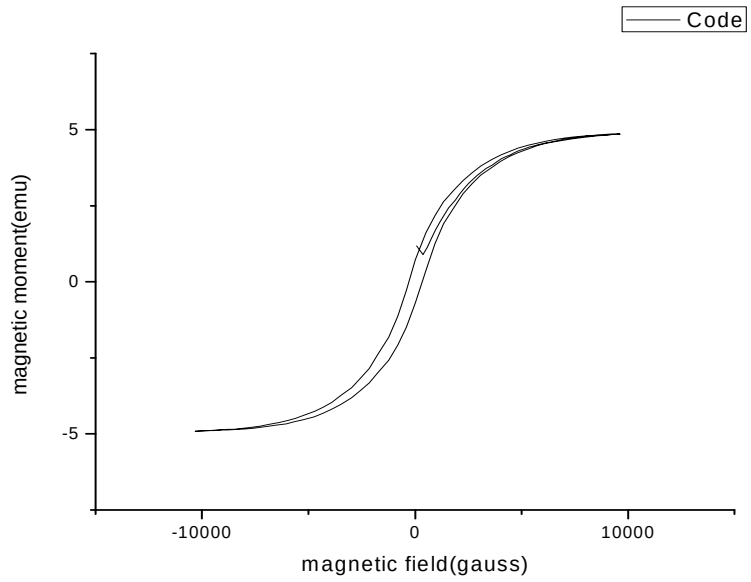

Fig 5.32 Graph between magnetic moment vs. magnetic field of 9 ton solid

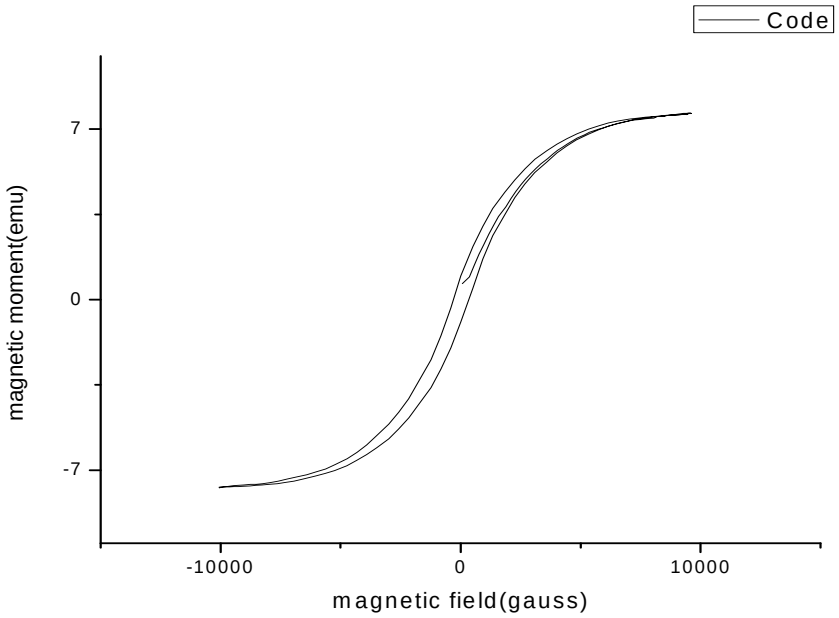

Fig 5.33 Graph between magnetic moment vs. magnetic field of 7 ton liquid

Chapter VII

Conclusions and Scope of Further Work

6.1 **conclusions and future work**

The present study on the powder processing, density, microstructure, micro hardness, SEM, XRD, VSM, and mechanical properties of Al_2o_3- CIP composite were undertaken to study the following.

1. The alumina and CIP based sintered magnetic abrasive powders were prepared by powder metallurgy method.

2. The micro hardness has been tested with micro hardness tester and result shows that micro hardness increases with load and higher sintering temperature.

3. The compressive stress value tested on UTM increases with compaction load and sintering temperature. The maximum value of compressive stress is 67.95 N/mm^2 at 9 ton liquid phase sintered sample.

4. Optical microscopy reveals that denser particles are obtained for higher compaction load.

5. XRD Shows crystalline structure and different phases present in the sample and lattice parameter. XRD study shows simple cubic, face cubic centred, and body cubic centred planes present in the sample. FWHM value of sample is 0.16°, 0.188°, 0.127°, and 0.174° respectively.

6. Scanning electron microscopy (SEM) analysis shows microstructure and size of particles has been seen diagonally on the micrograph to calculate the average particle size. Maximum size of particle in diagonal is 53.2 micron and average particle size is 29μ_m, 18.9μ_m, 24μ_m, 13μ_m respectively.

7. Magnetic properties of sintered abrasives have been studied by VSM. It has been found that the saturation magnetization increases with compaction load of pallets and sintering temperature.

Future work

The present study reveals that powder processing is an important step for achieving a dense microstructure. The magnetic abrasive will be used for finishing purpose in MAF, MRF and RMAF. Also improve the result of density and magnetic property of Al_2o_3 and CIP composites by vacuum sintering and compaction load. The magnetic abrasive will be used in aerospace and electronics industries for finishing of hard material which is not easy to finish by conventional method.

REFERENCES

1. D.W. Richer son, “The Magic of Ceramics”, Wiley- American Ceramic Society, USA (2000).

2. W.E. Lee and M. Rainferth, “Ceramic Microstructures: Property Control by Processing”, Chapman and Hall, Great Britain, 67-121 (1994)

3. Lenel, F.V. (1980). Powder metallurgy: Principles and applications. New Jersey, USA: Metal Powder Industries Federation

4. K. Nihara, “New Design Concept of Structural Ceramics: Ceramic Nano composites”, J. Ceram. Soc, Jpn 99, 974-982 (1991)

5. Rahimian, M. et al. (2009). “The effect of particle size, sintering temperature and sintering time on the properties of Al–Al2O3 composites, made by powder metallurgy.” Journal of Materials Processing Technology 209 (2009), 5387–5393.

6. Shamsuddin saidatulakmar et al.(2008) “ Characterization of Fe-Cr-Al_2O_3 Composites Fabricated by Powder Metallurgy Method with Varying Weight Percentage of Alumina” Journal of physical science 19(1), 89-95, 2008

7 .J. Tartaj and T. Tartaj (2002) “Preparation, characterization and sintering behaviour of Spherical iron oxide doped alumina particles” Acta Materialia 50 (2002) 5–12

8. LU C. Y. and HWANG S. K. (1999) “Densification of Carbonyl Iron Compacts by the Addition of Fine Alumina Powders” (1999)

9. Chen Lung Chih et al. (2002) “Sintering behavior and mechanical properties of nano-sized Cr3C2/Al2O3 composites prepared by MOCVI process” Journal of the European Ceramic Society 22 (2002) 2883–2892

10.Olevsky, Eugene A. (1997). “Theory of sintering: from discrete to continuum.”Materials Science and Engineering, R23 (1998), 41–100.

11. Park, H.H., Cho, S.J., Yoon, D.N.(1984)“Pore filling process in liquid phase sintering.”, Metallurgical transactions A, June 1984, 15(6) , 1075-1080.

12. R. L. Coble, ‘‘Sintering of crystalline solids I: Intermediate and final stage diffusion Models’’, J. Appl. Phys., 32, 787–792 (1961).

13. R. J. Brook, ‘‘Pore–Grain boundary interactions and grain growth’’, J. Am. Ceram. Soc., 52, 56–57 (1969).

14. E. A. Bar ringer and H. K. Bowen, ‘‘Formation, packing and sintering of monodispersed TiO_2 powders” J. Am. Ceram. Soc., 65, C199–201(1982).

15. C. P. Cameron and R. Raj, ‘‘Better sintering through green-state deformation processing’’, J. Am. Ceram. Soc., 73, 2032–2037 (1990).

16. A. Krell, P. Blank, H. W. Ha, T. Hutzler, and M. Nebelung, ‘‘Processing of High- Density Sub micrometer Al2O3 for New Applications,’’ J. Am. Ceram. Soc., 86, 546–53 (2003).

17. A. Krell and J. Klimke, ‘‘Effect of the homogeneity of particle coordination on Solid state sintering of transparent alumina’’, J. Am. Ceram. Soc., 89, 1985–1992 (2006).

18. W. H. Rhodes, ‘‘Agglomerate and particle size effects on sintering yttria- stabilized Zirconia’’, J. Am. Ceram. Soc., 64, 19–22 (1981).

19. T. S. Yeh and M. D. Sacks, ‘‘Effect of green microstructure on sintering of alumina’’; pp. 309–331 in Ceramics Transactions, Vol. 7, Sintering of Advanced Ceramics, Edited by C. A. Handwerkers, J. E. Blendell, and W. A. Kaysser. The American Ceramic Society, Westerville, OH, 1990.

20. F. F. Lange and B. J. Kellet, ‘‘Thermodynamics of densification, II. Grain growth in porous compacts and relation to densification’’, J. Am. Ceram. Soc., 72, 735–741 (1989).

21. K. G. Ewsuk, J. G. Arguello, D. N. Bencoe, D. T. Ellerby, S. J. Glass, D. H. Zeuch, and J. Anderson, ‘‘Characterizing powders for dry pressing, sintering’’, Bull. Am. Ceram. Soc., 82, 41– 47 (2003).

22. K. Maca, M. Trunec, and P. Dobsak, ‘‘Bulk zirconia nanoceramics prepared by cold isostatic Pressing and pressure less sintering’’, Rev. Adv. Mater. Sci., 10, 84– 88 (2005).

23. K. Matsui, I. N. Ohmich, M. Ohgai, M. Enomoto and J. Hojo, ‘‘Sintering kinetics at constant Rates of heating: Effects of Al2O3 on the initial sintering stage for fine zirconia powder’’, J. Am. Ceram. Soc., 88, 3346–3352 (2005).

23. G S Upadhyaya , 2002 “Powder Metallurgy Technology” Cambridge International Science publication, U.K

.